The role of wing mechanosensory feedback in insect flight control

Bradley H. Dickerson

A dissertation

submitted in partial fulfillment of the

requirements for the degree of

Doctor of Philosophy

University of Washington

2015

Reading Committee:

Thomas Daniel, Chair

Jeff Riffell

Bingni Brunton

Program Authorized to Offer Degree:

Biology

University of Washington

Abstract

The role of wing mechanosensory feedback in insect flight control

Bradley H. Dickerson

Chair of the Supervisory Committee:
Professor Thomas L. Daniel
Biology

Flying insects rapidly stabilize after perturbations using multiple sensory modalities (e.g., vision mechanoreception, olfaction) for active control. Mechanoreceptors' direct coupling of sensory structure to the environment, as opposed to the series of chemical cascades typical of photoreceptors, makes them critical components of locomotor control. For example, both dipteran (flies) and strepsipteran (twisted wing flies) insects possess pendular organs known as halteres that allow these animals to detect gyroscopic forces and correct for perturbations to the flight path. Yet, aside from the literature on halteres and recent work on the antennae of the hawkmoth *Manduca sexta*, it is unclear how other flying insects use mechanosensory information to control body dynamics.

In Chapter 1, I review the role of sensory input in insect flight control, particularly mechanosensory information. Evolutionarily derived from the wings, halteres are essential to

flight, providing information that allows flies to make rapid adjustments to their wing and body kinematics. During rotational maneuvers or instabilities during flight, halteres experience an inertial force that is orthogonal to the plane of oscillation, known as the Coriolis force. By definition, insect wings experience Coriolis forces during rotations. Further, the mechanosensory structures found on the halteres, campaniform sensilla, are also present on wings, suggesting that the wings can encode information about flight dynamics.

In Chapter 2 (Dickerson *et al.*, 2014), I test whether the wings can provide sensory information that helps informs the animal of its body dynamics. I use targeted manipulations of the wings to test for the presence of a reflex mediated by the embedded campaniform sensilla. I attach small rare-earth magnets to each wing and placed tethered moths within an electromagnet, thereby simulating an inertial stimulus around the animals' pitch axis. This stimulus elicits the same abdominal flexion reflex these animals exhibit in response to visual or whole-body pitch stimuli of the same frequency and amplitude. These results demonstrate that the wings can provide information about body dynamics during locomotion, a role previously thought to be the sole domain of the halteres.

In Chapter 3 (Eberle, Dickerson *et al.*, 2015), I use computational and robotic models of a flapping, flexible wing subject to rotation to address whether the Coriolis force can be experimentally observed using only changes in the wing's structural dynamics. I find that body rotation induces torsion that is the direct consequence of forces, including the Coriolis force, acting on the wings. I also find that this torsion changes the spatiotemporal pattern of strain across the wing. The emergent patterns of strain point to a mechanism by which flying insects could detect their angular velocity during perturbations or maneuvers via the structural dynamics of their wings.

In Chapter 4, I extend the method developed to stimulate the wings in tethered flight to test how wing mechanosensory information interacts with the visual system. I subject moths to a moving sinusoidal grating in both dim and near-total darkness conditions, testing moths' abdominal flexion response during visual stimulation alone and during simultaneous stimulation of the wings and visual system. I find no significant differences between the two groups at either light level, suggesting that moths will track a high contrast visual object, even in extremely dim conditions. My findings also support the wings' role as context-dependent sensory structures.

TABLE OF CONTENTS

LIST OF FIGURES

ACKNOWLEDGEMENTS

To make it this far in any endeavor is nigh impossible without a tremendous amount of support and mentorship. In my graduate experience, I have been lucky enough to work with Tom Daniel, a person who is unmatched in his thoughtfulness, kind heart, and collaborative nature. I met Tom three years before I entered graduate school, when I was picking up keys as a summer research student. Tom radiates an enthusiasm for science that impacts everyone he comes into contact with, and is always willing to teach lab members about both the technical aspects of science and how to navigate science as a career path. It has been a joy and an honor working with him on this project. Aside from Tom, I also owe a debt of gratitude to the members of my committee, Jeff Riffell, Bing Brunton, Sharlene Santana, and former member Michael Dickinson. You all pushed me new limits, and your advice and criticism helped make this project successful and graduate school an enjoyable experience.

Someone with Tom's personality has no trouble attracting dynamic people into his orbit, and the members of the Daniel lab past and present helped make this experience so rewarding. Thank you to Zane Aldworth, Armin Hinterwirth, Simon Sponberg, Jessica Fox, Eatai Roth, Bing Brunton, David Williams, Yonatan Munk, Jon Dyhr, Eric Rombokas, Sharri Zamore, Nicole George, Annika Eberle, Octavio Campos, Elischa Sanders, Jane Woods, and Darrin Howell. In addition to being great colleagues, many of you have also been great friends, and I will always hold dear our time together. Many thanks to members of the Dickinson lab, especially Peter Weir and Thad Lindsay for their help and advice. Thanks also to Pang Chan and Binh Nguyen.

Many thanks to Kaylan Brae Petrie, Rachel Merz, all my friends from the Secret Basketball Thread (particularly Patrick Lindsey and Seth Donoughe), the Potluck group, Jake Brunkard, Ariah Kidder, Andrew Matson, Austin Baird, Namdi Brandon, Catherine Lim, Cristina Hererra-Schrum, Christina Gasbarro, the Rap Internet and a whole lot of people for their friendship and support.

I would not be where I am today without the love and support of my parents and brother. I will never be able to stop saying thank you. Finally, to Holly, the person who has been my rock and best friend throughout this crazy trip: I love you more than you could ever know. Thank you.

Funding for this work was provided by a Graduate Opportunity Program Award, National Science Foundation Graduate Research Fellowship Program [no. DGE-0718124], the Air Force Office of Scientific Research [grant no. FA9550-11-1-0155], ONR MURI [grant no. N000141010952], DARPA HI-MEMS [no. FA8650-07-C-7704], and the University of Washington Komen Endowed Chair.

DEDICATION

For Mom-Mom and Avis

Chapter 1. INTRODUCTION

Animal locomotion involves a complex interplay between multiple structures across various levels of organization. Consider the incredible agility of flying insects. The large power muscles located in the thorax alternately contract in opposing directions, driving cyclic oscillations of the thoracic cuticle. The length changes induced by muscle contractions are transmitted via the composite material properties of the wing hinge to move the wings. The wings in turn conduct work on the surrounding fluid (air) environment, producing aerodynamic forces and moments. These forces change the insect's kinematics, which will change its sensory experience. Changes in the animal's sensory experience leads to changes in its motor output, restarting this closed feedback loop of behavior. This complex interaction and the relative experimental accessibility of insect nervous systems have made insect flight a prime model for the understanding of locomotor control (Wilson, 1961).

A central challenge in the study of insect flight, and animal locomotion more generally, is to understand how sensory information is transformed by the nervous system into a form upon which the motor system can act. The early stages of this transformation are common across all types of sensory receptors (i.e., photoreceptors, mechanoreceptors, and chemoreceptors) and is composed of multiple stages (Simmons and Young, 2010). First, energy from the stimulus must be coupled to the sensory receptor. This energy is then transduced by the sensory neuron of the associated receptor, converting the stimulus (i.e., light, kinetic energy, odor identity) into the currency of the nervous system, electrical energy. This electrical energy in many cases takes the form of action potentials, converting relevant information about the outside (or inner) world into

a code that can control behavior. Thus, an important component to the understanding of insects' aerial agility lies in the study of their various sensory structures.

Insect vision is easily the best-studied sensory modality in the context of flight control. Insect eyes are rigidly fixed to the head, visual processing centers dominate the volume of many insect brains, and vision's obvious role behaviors as diverse as foraging, mating, and obstacle avoidance make it a rich topic for study. However, many of the behaviors observed in free flight, such as the rapid right-angle turns in flies known as saccades, take place on time scales faster than known visual processing speeds (Bender and Dickinson, 2006a; Dickinson, 2005; Land and Collett, 1974). This is due in part to the method in which visual information is transduced by most photoreceptors; upon absorption of photons, a chemical cascade in the receptor is initiated, and the time lag between further processing and the final motor output lasts anywhere from tens to hundreds of milliseconds. Thus, flying insects must rely on multiple streams of sensory input to control complex behaviors.

An important sensory modality that along with the visual system enables rapid maneuvers in insect flight is mechanoreception. The sensory neurons of mechanoreceptors are directly coupled to the structures that allow them to detect kinetic energy imparted by the outside world or due to the animal's own movement. Thus, similar to the structural and optical properties of eyes, the mechanical properties of the wing, leg, or body act as the first level filtering for relevant stimulus information (Sane and McHenry, 2009). However, the transduction mechanism of mechanoreceptors is rather different from that of photoreceptors. Instead of a chemical signaling cascade, movement of the sensory structure is directly responsible for the opening of ion channels (French, 1988; Hudspeth, 1989; Walker et al., 2000). As a result, mechanoreceptors are exquisitely sensitive to motions of the sensory structures to which they are attached and

respond with latencies on the order of microseconds. In the context of insect flight, then, specialized mechanoreceptive organs can be used in concert other sensory modalities to reject perturbations and stabilize flight.

There is a long history of investigating the role of mechanoreception in insect flight control (Burrows, 1975; Derham, 1711; Gettrup, 1966; Pringle, 1948), much of which has come from the study of halteres, the gyroscopic organs of Diptera (true flies). Halteres are small club-shaped organs that sit behind the forewings and oscillate at wingbeat frequency, antiphase to the wings. During rotational maneuvers or instabilities during flight, halteres experience an inertial force orthogonal to the plane of oscillation (the Coriolis force) (Nalbach, 1993; Pringle, 1948). This force results in a strain at the base of the haltere, mediating compensatory reflexes through changes in wingbeat amplitude and frequency, as well as head and abdominal position (Dickinson, 1999; Nalbach and Hengstenberg, 1994; Sherman and Dickinson, 2003). These reflexes are attributed to the arrays of strain-sensitive campaniform sensilla and a chordotonal organ at the base of the haltere, with one field of these campaniforms (dF2) thought to be particularly important (Cole and Palka, 1982; Fayyazuddin and Dickinson, 1996; Fraenkel and Pringle, 1938; Gnatzy et al., 1987). Recent work has demonstrated that the haltere campaniform sensilla can encode a broad range of frequencies and exhibit extremely precise spike timing (Fox and Daniel, 2008; Fox et al., 2010), and flies that have the halteres removed do not respond to inertial stimuli (Dickinson, 1999), lending further support that these structures serve a gyroscopic function.

While the halteres' role in flight control is long established, they do not contribute to the production of aerodynamic force. Additionally, halteres are only found in two insect orders, Strepsiptera and Diptera. This invites the question as to how the vast majority of four-winged

insects collect information about their body dynamics. Recent studies suggest that the antennae of the hawkmoth *Manduca sexta* serve as proof masses for inertial sensing, and that mechanoreceptors at the base of each antenna are capable of encoding frequencies consistent with gyroscopic forces (Sane et al., 2007). Further, the antennae of *Manduca* mediate abdominal reflexes to inertial stimuli about the pitch axis (Hinterwirth and Daniel, 2010), their removal both eliminates the inertial reflex and compromises overall flight performance (Hinterwirth and Daniel, 2010; Sane et al., 2007), and stimulation of antennal muscles in freely flying *Manduca* initiates steering responses (Hinterwirth et al., 2012).

While this evidence implicates the antennae as inertial sensors, it does not exclude the possibility that other structures may play a similar role. For instance, consider that halteres are derived from the wings. Three lines of evidence suggest that wings themselves could function not only as actuators but also as inertial sensors. First, wing flapping combined with body rotations in planes orthogonal to the wing stroke will generate Coriolis forces, and the wings are subject to significant bending and torsion, primarily due to inertia (Combes and Daniel, 2003a; Ennos, 1988a; Lehmann et al., 2011). Second, wings, like halteres, are arrayed with a rich distribution of campaniform sensilla, particularly near the wing hinge (Cole and Palka, 1982; Gettrup, 1966). Finally, previous work on the wing campaniform sensilla of flies and *Manduca* show the ability to encode a broad range of frequencies, much like the halteres (Daniel et al., 2012; Dickinson, 1990a). Thus, by actuating the wing, a flying insect would be able to detect information during flight that would be otherwise unavailable. Indeed, in his seminal study on the structure and function of the haltere, Pringle (Pringle, 1948) noted that it is unlikely that the haltere evolved *de novo*, and it is therefore possible that the campaniform sensilla embedded in the wings of other flying insects help control maneuvers. Alternatively, the evolution of the

haltere could reflect the existence of a tradeoff between sensing and actuation, the evolution of functional diptery (as in Hymenoptera or Lepidoptera), or other constraints. Regardless, the extent to which the dynamics of a moving actuator interact with its sensor distribution to encode behaviorally relevant stimuli has remained relatively unexplored. In this dissertation, I use a combination of engineering, neuroscience, and behavioral techniques to examine the potential for insect wings to serve as sensors of body dynamics.

1.1.1 *Moth flight posture is mediated by wing mechanosensory feedback*

To test whether the wings can provide sensory information that helps informs the animal of its body dynamics, in Chapter 2 I use a combination of anatomy, intracellular electrophysiology and targeted manipulations of the wings. I show that the neurons innervating these sensilla on the forewings of *M. sexta* exhibit spike-timing precision comparable to that seen in previous reports of campaniform sensilla, including haltere neurons. I then attach small rare-earth magnets to each wing and placed tethered moths within a rotating electromagnet, thereby simulating an inertial stimulus around the animals' pitch axis. By subjecting these animals to a rotating magnetic field during tethered flight, I elicited the same vertical abdominal flexion reflex these animals exhibit in response to visual or whole-body pitch stimuli of the same frequency and amplitude. These results demonstrate that the wings can provide information about body dynamics during locomotion, a sensory role predicted nearly seventy years ago.

1.1.2 *A new twist on gyroscopic sensing: body rotations lead to torsion in flapping, flexing insect wings*

Insect wings are flexible structures that experience Coriolis forces as they undergo rapid rotational accelerations during flight. The spatiotemporal patterns of wing during these maneuvers or perturbations in turn affect the firing of embedded mechanoreceptors, leading to changes in body posture and thus body dynamics. But can the Coriolis force be experimentally observed using only changes in the structural dynamics of a flapping flexible wing?

In Chapter 3 I build robotically actuated models to rotate a flapping wing about an axis orthogonal to flapping to measure the displacement of the model wing's free ends and the strain near the base of the wing. I find that body rotation induces a new dynamic mode: torsion. This torsion is the direct consequence of forces, including the Coriolis force, acting on the wings. I also find that this torsion induces a strain across the wing that is greatest at the wing base. In the context of a flapping insect wing, this strain could stimulate the campaniform sensilla embedded in the wing and thereby trigger compensatory reflexes. These results point to a mechanism by which flying insects could detect their angular velocity during perturbations or maneuvers via the structural dynamics of their wings.

1.1.3 *Visual information attenuates wing-mediated mechanosensory feedback in the hawkmoth* Manduca sexta

The control of insect flight is mediated by the interaction of multiple sensory modalities including, but not limited to, visual and mechanosensory information. For instance, the halteres of flies are mechanosensory organs that encode inertial forces that, in concert with the visual system, aid rapid course correction during flight. Yet, it is unclear how the vast majority of all

other flying insects use multimodal sensing to control body dynamics.

In Chapter 4 I extend the method developed in Chapter 2, subjecting moths to a pitch stimulus *via* magnetic wing perturbations in combination with a visual pattern during tethered flight in dim light and near-total darkness, conditions consistent with the crepuscular periods during which moths are most active. Surprisingly, I find no difference in abdominal reflex gain when moths are subject to combined visual and wing mechanosensory stimuli compared to visual stimuli alone. These results suggest that in the presence of high contrast objects, moth flight control circuitry is dominated by the visual system, and the role of wing mechanosensory feedback is context-dependent.

Chapter 2. CONTROL OF MOTH FLIGHT POSTURE IS MEDIATED BY WING MECHANOSENSORY FEEDBACK

Bradley H. Dickerson, Zane N. Aldworth and Thomas L. Daniel
The Journal of Experimental Biology (2014) 217, 2301-2308 doi:10.1242/jeb.103770

Flying insects rapidly stabilize after perturbations using both visual and mechanosensory inputs for active control. Insect halteres are mechanosensory organs that encode inertial forces to aid rapid course correction during flight but serve no aerodynamic role and are specific to two orders of insects (Diptera and Strepsiptera). Aside from the literature on halteres and recent work on the antennae of the hawkmoth *Manduca sexta*, it is unclear how other flying insects use mechanosensory information to control body dynamics. The mechanosensory structures found on the halteres, campaniform sensilla, are also present on wings, suggesting that the wings can encode information about flight dynamics. We show that the neurons innervating these sensilla on the forewings of *Manduca* exhibit spike-timing precision comparable to that seen in previous reports of campaniform sensilla, including haltere neurons. In addition, by attaching magnets to the wings of moths, and subjecting these animals to a simulated pitch stimulus *via* a rotating magnetic field during tethered flight, we elicited the same vertical abdominal flexion reflex these animals exhibit in response to visual or inertial pitch stimuli. Our results indicate that, in addition to their role as actuators during locomotion, insect wings serve as sensors that initiate reflexes that control body dynamics.

2.1 INTRODUCTION

Flying insects require mechanosensory information to reject environmental perturbations and execute maneuvers. While visual input is crucial for maintaining stability (Dyhr *et al.*, 2013), the transduction and processing speeds of most insect visual systems may be too slow to account for the rapid behaviors observed in free flight (Land and Collett, 1974; Theobald *et al.*, 2010). Thus, insects combine visual input with extremely fast and precise mechanoreception (Bender and Dickinson, 2006b; Fayyazuddin and Dickinson, 1996; Hinterwirth and Daniel, 2010; Huston and Krapp, 2009; Pix et al., 1993; Sherman and Dickinson, 2004) to navigate through complex, unpredictable environments.

True flies (Diptera) and twisted-wing insects (Strepsiptera) show convergent evolution of an elegant solution for sensing body rotations in the mechanosensory organs known as halteres. Evolutionarily derived from wings, halteres are paired, club-shaped structures located next to the wings that oscillate during flight; they use spatially distributed mechanosensors (campaniform sensilla) to precisely detect linear or rotational accelerations, triggering correctional flight maneuvers (Derham, 1711; Dickinson, 1999; Fayyazuddin and Dickinson, 1996; Fraenkel and Pringle, 1938; Nalbach and Hengstenberg, 1994; Pringle, 1948; Sherman and Dickinson, 2003). During rotational maneuvers or instabilities during flight, halteres experience an inertial force that is orthogonal to the plane of oscillation (the Coriolis force), the detection of which mediates these compensatory reflexes (Dickinson, 1999; Nalbach and Hengstenberg, 1994; Pringle, 1948; Sherman and Dickinson, 2003). Yet while halteres are actuated structures, they serve no known aerodynamic function and are only found in these two insect orders (Pix *et al.*, 1993).

Recently, the antennae of *Manduca sexta* have been implicated in inertial sensing, with the mechanoreceptors at the base of each antenna mediating abdominal reflexes to mechanical pitch

stimuli (Hinterwirth and Daniel, 2010; Sane *et al.*, 2007). During this reflex, moths vertically flex the abdomen in response to an inertial pitch stimulus, adjusting the center of lift relative to the center of mass (Dyhr *et al.*, 2013). Moreover, removal of the antennae both eliminates the inertial reflex and compromises overall flight performance (Hinterwirth and Daniel, 2010; Sane *et al.*, 2007). But aside from these two examples of insects using inertial sensing to aid flight control (and the head of dragonflies as a detector of roll; (Mittelstaedt, 1950), it remains a long-standing question as to how most flying insects collect mechanosensory information to control body dynamics.

Although experimental evidence implicates the antennae of *Manduca* as inertial sensors, it does not preclude other structures from serving similar roles. The halteres are evolutionarily derived from wings and the two possess the same sensory structures, campaniform sensilla. Perhaps then the evolution of gyroscopic sensing could have predated the development of the halteres. Alternatively, the campaniform sensilla embedded in the wings could detect other forces that the wings experience, including aerodynamic and inertial-elastic forces, or the mechanical state of the wing after collision events or damage. Early work in the desert locust *Schistocerca gregaria* demonstrated that ablation of the campaniform sensilla on the hindwings has important behavioral consequences, disrupting the control of twist in the forewings and disabling the animal's ability to produce lift or thrust (Gettrup, 1965; Gettrup, 1966; Gettrup and Wilson, 1964). Later experiments examining how the campaniform sensilla of the hindwing respond to wing twisting found them most responsive to strain magnitude during wing supination, providing input to motor neurons that control the flight muscles (Elson, 1987). Similar results showing the importance of feedback from wing campaniform sensilla regulating the timing of flight muscle contraction has been studied in flies (Heide, 1979; Heide, 1983).

While previous research highlights the importance of wing proprioceptive input during flight, the wings of modern insects may retain the ability to initiate reflexes that control body dynamics in a manner similar to the visual or inertial sensory systems (Dyhr *et al.*, 2013; Hengstenberg, 1988; Hinterwirth and Daniel, 2010; Pix *et al.*, 1993). To explore this issue, we combined anatomical, electrophysiological, and behavioral studies and determined that the wings of *Manduca* can indeed function as sensors that induce steering reflexes, suggesting that the capacity to use wings as sensory structures may be common to most flying insects.

2.2 MATERIALS AND METHODS

2.2.1 *Animals*

Manduca sexta (Linneaus) were raised in the Department of Biology at the University of Washington, Seattle. For SEMs and determining locations of distal wing campaniform sensilla, we used 16 male and 8 female moths that were between 1-8 days post-eclosion. For electrophysiological experiments we used 3 male and 4 female moths 1-5 days post-eclosion. For experiments using a simulated mechanical stimulus, we used 4 male moths 1-3 days post-eclosion.

2.2.2 *Mapping campaniform sensilla/SEMs*

We examined each moth to ensure that the wings had not sustained any significant damage. After identifying sex and day of eclosion, we excised a single forewing from one side after anesthetizing the animal by chilling it in a refrigerator for 15 min. We used wings from 14 male

and 7 female moths. We then removed the scales using damp Kimwipes and cotton swabs. We mounted wings between two microscope slides using glycerol, viewed them under a dissecting microscope, and recorded locations of the wing campaniforms on pictures of a *Manduca* wing. For scanning electron micrographs (SEMs), after chilling and excising each wing sample (2 male and 1 female), we removed and descaled the wing base and desiccated it overnight. We then mounted, sputter-coated in gold (Hummer V: Au target, Technics, San Jose, CA) and viewed each sample with a scanning electron microscope (JSM-840A, JEOL, Tokyo).

2.2.3 *Electrophysiology and jitter analysis*

We recorded intracellularly from the axons of afferent neurons innervating the campaniform sensilla on the dorsal and ventral surfaces of forewing nerve IINc1 (Nüesch, 1957). We pulled sharp intracellular electrodes from quartz capillary tubes using a model P2000 Micropipette Puller (Sutter Instruments Co., Novato, CA). We filled electrodes with 3M KCl, with resultant resistances of between 10 and 30 MΩ. We monitored membrane potential using an Axoclamp-2B amplifier (Molecular Devices, Sunnyvale CA), sampling membrane and stimulus voltage at 10 kHz and recorded on a Windows platform using the MATLAB data acquisition toolbox. We stimulated the wing by attaching a model 322C length controller (Aurora Scientific, Aurora ON) directly to the wingtip. We supplied pre-built stimulus voltages from a Windows computer to the servo-lever system. Stimuli consisted of between ten and fifty repeats of Gaussian White Noise (GWN) mechanical stimulation band-limited to 10-200 Hz, with RMS amplitude of 3.8 mm at the wingtip, which is about an order of magnitude lower than the base-to-tip excursions experienced by the wing during a normal wingstroke (8.5 cm). A standard deviation of 3.8 mm was the maximum our setup allowed in order to maintain a linear voltage to wingtip distance

relationship.

We identified single-spike events that were consistently elicited by repeated presentations of the stimulus with a modified version of the event identification protocol of Yen *et al.* (Yen *et al.*, 2007). First, in order to avoid results due to including data in which the cell was adapting, we excluded initial repetitions of the stimulus where the firing rate averaged across the repetition differed by more than 20% from the average firing rate across all trials. We then binned the adapted responses to repeated trials of the stimulus into histograms at a 1-msec resolution, and set a threshold at 30 times the mean firing rate in order to define firing boundaries of events. We determined from the collections of all events in the data set the events that consisted of single spikes with no contaminating spikes in a 20-msec window around the event for at least 20% of the trials. We note that varying this exclusion between 10 and 90% of the trials did not greatly affect the jitter analysis. For each event, we extracted the timing of the spike on each trial, and calculated the jitter as the standard deviation of the event time across trials (Mainen and Sejnowski, 1995).

2.2.4 *Helmholtz coils*

We used a pair of Helmholtz coils (U8481500, American 3B Scientific, Atlanta, GA) mounted to a stepper motor that has been described previously (Hinterwirth and Daniel, 2010) Figure 2.4A). The Helmholtz coils were 150 mm apart and each coil had a mean radius of 150 mm (inner radius: 287 mm, outer radius: 311 mm). We controlled the stepper motor through a custom Arduino script that generated a 20° (peak-to-peak), 3 Hz sinusoid about the pitch axis, that was converted into 0.2° steps by a micro-step controller (G201, GeckoDrive Inc., Tustin, CA, USA). To track the motion of the Helmholtz coils, we attached an infrared LED to the coils.

We powered the coils with 5A and 7.25V, resulting in a constant field strength of approx. 3.8 mT.

2.2.5 *Animal preparation for magnetic field wing perturbations*

All behavioral experiments rely on the abdominal flexion that occurs in response to open-loop visual and mechanical pitch rotational stimuli (Dyhr *et al.*, 2013; Hinterwirth and Daniel, 2010). We suspended each moth in the Helmholtz coils by attaching them *via* a ventral tether to a stable platform in between the coils. To do so, we chilled each moth in a refrigerator for 20 min. and glued a ventral tether between the mesothoracic and metathoracic segments. We dark-adapted each moth for 20 min. before beginning trials. We conducted all experiments in near total darkness and illuminated moths with infrared LEDs. We recorded three trials per treatment per moth with a high-speed camera (100 fps, 400 μs shutter, Phantom Miro, Vision Research, NJ). We conducted analyses only on trials that consisted of at least 10 sec of continuous flight.

In the first set of experiments, we tested the ability of *Manduca* to detect magnetosensory information as seen in monarch butterflies (*Danaus plexippus*; (Merlin et al., 2009) by powering the coils and rotating them around tethered flying moths. After these controls, we again chilled moths and placed a pair of small rare-earth magnets (mass: 13 mg, diameter: 1.6 mm, height: 0.8 mm; Magcraft NSN0591) between the first and second medial veins of each forewing, with the wing in between the attracted magnets (Fig. Figure 2.2D, black circles). For comparison, the mass of a typical *Manduca* wing is 42 mg. We mounted the magnets distal to the wing base, and approximately 2.5 mm from the wing's leading edge. We positioned the magnets to ensure that the polarity was the same for both wings and for all animals. We allowed moths to dark-adapt after 20 min., and ran trials in both the presence and absence of the magnetic field.

2.2.6 *Analysis of perturbation data*

We digitized videos of moths placed in the Helmholtz coils with DLTdv5 (Hedrick, 2008), using the penultimate abdomen segment, tether, and LED as points of interest. Using a custom MATLAB script (The MathWorks, Natick, MA), we computed the angular position of the coils (stimulus), θ_c, and the abdomen (response), θ_a, following the convention of Dyhr *et al.* (Dyhr et al., 2013) Fig. Figure 2.4A). We subtracted the mean of θ_a to remove linear trends from the data, and then performed Discrete Fourier Transforms of the stimulus and response to calculate the gain and phase of the abdominal reflex at the driving frequency of 3 Hz. The gain of the response, $G(f)$, is defined as the frequency-dependent ratio of the response amplitude to the stimulus amplitude. The phase of the response, $\theta(f)$, is defined as the difference in time lag normalized to the period length. We implemented repeated measures ANOVAs and two-sample t-tests in MATLAB on the calculated gain values.

2.2.7 *Calibration of wing perturbation stimulus*

To obtain an estimate of the stimulus applied to the wings by the Helmholtz coils, we measured the torsional stiffness of the *Manduca* wing as well as the amount of induced torsion to the wings caused by the magnets when the Helmholtz coils rotated. To measure torsional stiffness, we collected 7 1-3 day post-eclosion males and anesthetized each animal by chilling them in a refrigerator for 15 min. We then excised the left forewing of each animal. We clamped the wing to a micromanipulator, lowering it onto an insect pin that we placed on a scale (Mettler PL200, Hightstown, NJ, USA). We lowered each wing such that the first cubital vein was lightly

touching the insect pin at the start of the measurement. We then measured the moment arm from the first cubital vein to the wing's point of attachment at the micromanipulator. We recorded vertical displacement of the wing and the mass applied to the pin. We recorded eight measurements per wing; we first lowered the wing onto the pin by 200 μm, then by 100 μm increments for each subsequent measurement. After each trial, we measured the length from the leading edge of the wing to the first cubital vein. From this length and the vertical displacement, we calculated the angle to which the wing had been twisted, and calculated the torque on the wing by multiplying the measured mass applied to the pin by the acceleration due to gravity, and the measured moment arm. We performed a linear regression on each measurement of torque *versus* angle to obtain the torsional stiffness for each wing. From these measurements, we obtained a torsional stiffness of 2.17 ± 0.98 μN*m/deg (Fig. Figure 2.1). To estimate the torsion applied to the wings by the rotating magnetic field, we attached magnets to the excised wings of 5 1-3 day-old post-eclosion moths. We used 3 males and 2 females. We taped wings to a tether and rotated the powered Helmholtz coils for 10s around the wings in two different trials: at 0° and 45° with respect to horizontal. We recorded each trial at the same frame rate and shutter speed as the behavioral experiments. We observed a maximum deflection of ± 0.3° at 3Hz of the trailing edge of the wings, suggesting that a still wing experiences approximately a 650 nN*m torque. This amount of torque is approximately 10 times larger than the expected torque for a plate with the same moment of inertia as a *Manduca* wing rotating 20° (peak-to-peak), at 3 Hz. It is important to note that this torque estimate does not take into account wing motion relative to that of the Helmholtz coils, but is probably much smaller than the torques associated with normal *Manduca* wingbeat kinematics.

2.3 RESULTS

2.3.1 *Manduca forewings possess campaniform sensilla*

Manduca forewings are richly equipped with campaniform sensilla dorsally and ventrally (Figure 2.2), with concentrations of sensilla at the wing base. On the dorsal surface, five groups of campaniform sensilla are found at the base of the radial wing vein (Figure 2.2B); on the ventral surface, two to three groups are found at the base of the ventral subcostal wing vein (Figure 2.2C). Distally along the wing, approximately 45 campaniform sensilla can be found on the dorsal and ventral surface (Figure 2.2D, blue circles). In all, nearly 250 campaniform sensilla are found on each *Manduca* forewing, comparing favorably to the number found on the wings (between 120-154 campaniforms) and halteres (338 campaniforms) of the blowfly *Calliphora vicina* (Gnatzy *et al.*, 1987) and is close to four times the number found on the hindwing of the locust *Schistocerca gregaria* (Gettrup, 1965).

2.3.2 *Manduca forewing campaniform sensilla exhibit high spike-timing precision*

A general feature of campaniform sensilla afferents (Chapman et al., 1979; Dickinson, 1990b; Dickinson, 1990a; Fox et al., 2010) which is also thought to be important to flies' sensitivity to rapid inertial perturbations (Dickinson, 1999; Sherman and Dickinson, 2003), is the ability to precisely encode mechanical stimuli across a broad range of frequencies. We therefore performed intracellular recordings from the forewing nerve of *Manduca* while mechanically stimulating the wing with band-limited Gaussian noise (10-200 Hz) with a motorized lever arm to confirm such abilities for *Manduca* campaniform afferents (Figure 2.3A-C). There are numerous ways to describe how stimulus input is transformed into neuronal output. These

methods include calculating the coherence between the stimulus and response (Borst and Theunissen, 1999), the spike-triggered average (STA; (Dickinson, 1990b), or looking at higher order features of the STA (Fox *et al.*, 2010). However, we sought a concise, quantitative metric that would allow us to compare *Manduca* campaniform afferents to previous reports of other insects. We thus calculated the standard deviation of spike arrival time (*i.e.*, jitter) at specific stimulus events as a measure of timing precision (Mainen and Sejnowski, 1995). The jitter value for half of the spiking events across all animals was less than 0.60 ms (median jitter = 0.52 ms, mean ± 1 s.d. = 1.02 ± 1.04 ms; Figure 2.3D-E). This jitter value is nearly 10 times smaller than the period of the highest frequency component of the stimulus and close to 80 times smaller than the *Manduca* wingbeat period of 40 ms, indicating that the neurons innervating the wing campaniforms were capable of precisely encoding mechanical stimuli across a broad range of frequencies.

2.3.3 *Perturbation of the wings during tethered flight induces compensatory reflexes*

To determine whether mechanosensory input from *only* the wings could contribute to flight control, we attached small (13 mg) rare-earth magnets on the wings of tethered, flying *Manduca* (Figure 2.2D, black circles) and placed the moths inside of a rotating magnetic field (strength: 3.8 mT; approximate torque: 650 nN*m, see Methods) produced by a pair of Helmholtz coils (Figure 2.4A). To minimize visual input from the rotating coils, we conducted all experiments in near-dark conditions. We stimulated moths about the animals' pitch axis with a stimulus that is nearly 10 times larger than when *Manduca* are subject to whole-body mechanical pitch rotations at the same frequency and amplitude (Hinterwirth and Daniel, 2010), using three 10 s trials of a 20° (peak-to-peak), 3 Hz sinusoid rotation of the coils.

To determine the efficacy of the wing mechanical perturbation in eliciting the abdominal reflex, we measured moths' abdominal angle, θ_a as a function of time and compared it to the angle of the Helmholtz coils, θ_c (Figure 2.4B).

First we tested *Manduca*'s visual response to the rotating coils in the absence of a magnetic field (no power to the coils). Even in low light conditions, *Manduca* with magnets on their wings showed moderate abdominal flexion in response to the visual signal of rotating Helmholtz coils (Figure 2.4C, black line). A Fourier Transform of both θ_c and θ_a reveals a sharp peak at the driving frequency of 3 Hz of the pitch stimulus produced by the rotating coils (Figure 2.4D). We used the real and imaginary components of the Fourier Transforms to determine the gain and phase of the abdominal response. In 12 trials of 4 moths, the mean gain was 0.121 ± 0.092 with a phase of −49.76° ± 29.17° (mean ± circular s.d.).

To exclude the possibility that *Manduca* were sensitive to the magnetic field produced by the Helmholtz coils, we performed an additional behavioral assay in which we removed the magnets from the wings and observed moths' responses to rotating and powered Helmholtz coils. *Manduca* responses to the rotating coils in the presence of a magnetic field without placing magnets on the wings were not significantly different from moths with magnets in the unpowered coils (gain: 0.115 ± 0.101; phase: -50.53° ± 15.88°; N = 5 trials, 3 moths; two-sample t-test gain: P = 0.902). We thus pooled these data for comparison with wing perturbation experiments.

To experimentally test the hypothesis that the wings of *Manduca* serve as both actuators and sensors to control body dynamics, perturbation of only these structures during flight should result in a compensatory abdominal reflex. Thus we performed a third experimental treatment in which we attached magnets to the wings of moths experiencing tethered flight in rotating, powered

Helmholtz coils. In 9 trials of 3 moths, *Manduca* tested with magnets on their wings displayed strong abdominal reflexes in response to the rotating coils in the presence of a magnetic field (Figure 2.4C, magenta line) and there is a strong 3 Hz component to θ_a (Figure 2.4D). Each moth responded differently to both the visual stimulus of the rotating coils alone and the dynamic torque stimulus (Figure 2.4E). Accordingly, we observed a significant effect of individual moths on the gain of the abdominal response in each experimental treatment (coils off: $P < 0.05$; coils on: $P < 0.05$; repeated measures ANOVA; Figure 2.4E). In spite of this variability between animals, a polar plot (Figure 2.4E) shows that wing perturbation induced significantly stronger abdominal reflexes than the visual signal of the rotating coils alone (gain: 0.354 ± 0.164, phase: -67.31 ± 10.30°; $P < 0.05$; repeated measures ANOVA; N = 12 trials, 4 moths). We saw no effect of trial number or the interaction between trial number and experimental treatment (data not shown).

2.4 DISCUSSION

This research was motivated by the notion that wings, as the evolutionary precursors to the gyroscopic sensory organs of Diptera (halteres), could provide mechanosensory information that is involved in flight control. Moreover, sensory information would be encoded by campaniform sensilla similar to previous studies of these sensory structures. Accordingly, we were able to show that the wings of *Manduca* have campaniform sensilla distributed over the wing blade and in patches at the base of the wing. In addition, neural recordings indicate that these sensory cells are capable of rapidly and precisely encoding mechanical stimuli. Importantly, direct perturbations to the wings *via* a magnetic field rotating in the pitch axis causes compensatory reflexes similar to those elicited by both visual pitch stimuli and entire body rotations

(Hinterwirth and Daniel, 2010). The evolution of the haltere, with its reduced size and knob-like shape that generates negligible lift and drag forces during flight, allows true flies and strepsipterans to detect inertial forces independent of aerodynamic loading. In contrast, the wings of large insects like *Manduca sexta* clearly generate aerodynamic forces and, as we show, also detect wing bending dynamics. Thus, wings could serve the dual role of both sensor and actuator. That is, by actuating the wing, a flying insect could detect information during about its body dynamics that would be otherwise unavailable without flapping, such as the Coriolis force associated with body rotations or different wing bending dynamics between the wings due to aerodynamic loading.

2.4.1 *Temporally precise campaniform sensilla are embedded in Manduca forewings*

The inertial reflexes observed in flies, such as changes in wing kinematics, head position, or abdominal position in response to imposed whole-body rotations (Dickinson, 1999; Hengstenberg, 1988; Nalbach and Hengstenberg, 1994) are largely attributed to the arrays of strain-sensitive campaniform sensilla found at the base of each haltere (Bender and Dickinson, 2006b; Chan and Dickinson, 1996; Dickinson, 1999; Fayyazuddin and Dickinson, 1996; Fraenkel and Pringle, 1938; Gnatzy et al., 1987; Hengstenberg, 1988; Nalbach and Hengstenberg, 1994; Sherman and Dickinson, 2003; Sherman and Dickinson, 2004). These sensilla are also found on the wings of other insects (Diptera: Cole and Palka, 1982; Lepidoptera: Dombrowski, 1991; Orthoptera: Gettrup, 1965; Gettrup, 1966; Gnatzy et al., 1987; Ando:2011jb; Hemiptera: Zacwilichowski, 1931), including *Manduca* (Figure 2.2).

A general feature of the neurons innervating these sensilla, in conjunction with the structural specialization of the campaniform sensilla dome (Fox et al., 2010; Fraenkel and Pringle, 1938;

Gnatzy et al., 1987; Pringle, 1948), is the sub-millisecond spike-timing precision of the afferents (Chapman et al., 1979; Dickinson, 1990b; Dickinson, 1990a; Fox et al., 2010). Our recordings from afferent neurons innervating *Manduca* wing campaniform sensilla show that these neurons exhibit a level of spike-timing precision similar to values observed in fly halteres (Fox and Daniel, 2008).

Halteres experience large inertial-elastic forces in their plane of oscillation (Nalbach, 1993). As a fly rotates in an axis orthogonal to that of the halteres, they experience a Coriolis force that is much smaller than the inertial in-plane forces (Nalbach, 1993). Previous work (Fox *et al.*, 2010; Pringle, 1948) has suggested that detecting the small, out-of-plane motions that arise from the Coriolis force requires high temporal precision. Moreover, the importance of proprioceptive feedback from the campaniform sensilla on wings and halteres for regulating normal wingstroke kinematics has long been known (Fayyazuddin and Dickinson, 1999; Heide, 1979; Heide, 1983). Our electrophysiological results suggest that the forewing campaniform sensilla exhibit sufficient precision for both proper wingstroke maintenance as well as detecting rapid changes in body dynamics or wing bending.

2.4.2 *Wing campaniforms provide sensory feedback to abdominal response*

The above morphological and electrophysiological evidence suggests that wings could provide information relevant to flight control. However, confirmation of such a role would require demonstrating that perturbing *only* the wings, and leaving the rest of the animal undisturbed, mediates a reflex similar to the abdominal movements observed in response to a mechanical pitch stimulus (Hinterwirth and Daniel, 2010). Our preparation allowed us to provide the wings with just such a dynamic torque stimulus while leaving the rest of the animal

unperturbed. While we were unable to determine the detailed effects of our preparation on wing kinematics or wing strain patterns, by comparing responses of moths in this system with the coils on or off we were able to clearly identify the responses due to a mechanical stimulus provided solely to the wings (Figure 2.4).

Studies on the role of inertial sensing in insect flight have typically looked at responses to whole body rotations as well as the impact of sensor ablation (Bender and Dickinson, 2006b; Dickinson, 1999; Hengstenberg, 1988; Hinterwirth and Daniel, 2010; Nalbach and Hengstenberg, 1994; Pix et al., 1993; Sane et al., 2007; Sherman and Dickinson, 2003; Sherman and Dickinson, 2004; Viollet and Zeil, 2013). The primary drawback of testing the effect of campaniform ablation with our experimental setup is the technical challenge of eliminating each of the nearly 250 campaniform sensilla per wing. These structures are micron-scale in size, and thus extremely difficult to ablate without potentially damaging the rest of the wing. Additionally, this experimental approach does not account for the contributions of other potential inertial sensors. Aside from technical limitations, inertial sensors such as the halteres are not only responsible for measuring body rotations, but the regulation of normal wing kinematics as well, similar to wing campaniform sensilla (Gettrup, 1966; Heide, 1983). Given the multiple roles of mechanosensory feedback in the regulation of flight locomotor patterns, then, interpreting the results of ablation experiments is rather difficult. Further, only a few experiments have looked for compensatory reflexes as a direct result of manipulating putative inertial sensors (Hinterwirth *et al.*, 2012). To our knowledge, this is the first demonstration that the wing campaniform sensilla induce reflexes involved in the control of body dynamics, a sensory role predicted by Pringle (Pringle, 1948; Pringle, 1957). Our findings that wing pitch perturbations in *Manduca* elicit an abdominal reflex are also consistent with the effect of virtual pitch rotations on the

blowfly *Calliphora erythrocephala* (Nalbach and Hengstenberg, 1994) and the effect of yaw rotations on the strepsipteran *Xenos vesparum* (Pix *et al.*, 1993).

The 3 Hz pitch stimulus from a rotating magnetic field drove wing perturbations that resulted in a much larger abdominal response (35-fold increase) than *Manduca* subject to whole body pitch rotations at the same driving frequency and amplitude (Hinterwirth and Daniel, 2010). This large difference in the strength of the abdominal responses observed in this study compared to those reported by Hinterwirth and Daniel (2010) is likely due to our targeted perturbations subjecting the wings to torques an order of magnitude larger than would be experienced by whole body rotations of the same amplitude and frequency, eliciting larger abdominal excursions. Previous work on the inertial sensing capacities of the halteres and antennae suggests that these structures act as high-pass filters, such that the stronger the rotational input, the stronger the behavioral response (Hinterwirth and Daniel, 2010; Sherman and Dickinson, 2003). Thus, the wing torques experienced during the whole body rotations used by Hinterwirth and Daniel, whether due to aerodynamic or inertial forces, might have been too low to excite the wing-mediated abdominal response. Our results provide strong evidence that forces acting on the wings that are likely small relative to the normal patterns of aerodynamic and inertial forces and moments produced are closely monitored by the nervous system and provide information relevant to control.

Using the wings as sensory structures in flight may introduce sensory noise from wing bending due to inertial-elastic effects that could limit the capacity for *Manduca* to detect and respond to inertial stimuli (Combes and Daniel, 2003a). It remains unclear if the frequency bandwidth of the compensatory reflex in *Manduca* is limited, at least compared to insects with halteres. However, *Manduca* is much larger than both dipteran and strepsipteran species and, due

to its greater inertia, may not require the sensory bandwidth (at higher frequencies) needed for smaller insects. Alternatively, mechanosensory information from the wings could be combined with inertial information from the antennae, a previously established gyroscopic sensor in *Manduca*, potentially remedying any signal-to-noise issues. This interaction between mechanosensory sensing mechanisms may explain why *Manduca* that had their antennae removed were unable to sustain stable flight (Sane *et al.*, 2007). The antennae may act as the primary inertial sensor in *Manduca*, with the wings providing additional information to control body dynamics. Further experiments that address the extent to which information from wing campaniform sensilla is used in conjunction with the antennae along with other modalities will provide a better understanding of the wings' sensory capacity and influence over body dynamics.

2.4.3 *Can wings separate aerodynamic and inertial forces?*

Though it is tempting to interpret our data as implicating the wings as sensors of rotational body dynamics similar to the halteres, the arrangement of campaniform sensilla distal to the wing base (Figure 2.2D) suggests that the wing campaniform sensilla control abdominal reflexes arising from the detection of wing bending due to multiple different forces. During flapping, insect wings undergo large bending and torsion (Wootton, 1981a; Wootton, 1992). Whereas aerodynamic and inertial forces are thought to contribute nearly equally to wing bending for flies (Ennos, 1988b; Lehmann et al., 2011), a combination of computational and experimental techniques have suggested that wing bending in *Manduca* may be due mostly to inertial-elastic, rather than aerodynamic, loading (Combes and Daniel, 2003a; Daniel and Combes, 2002). Thus, the amount of bending an insect wing undergoes is likely a function of a combination of wing stiffness, flapping frequency, aerodynamic loading, and inertial forces. Nonetheless, a model

comparing aerodynamic, inertial-elastic, and Coriolis forces in a flapping wing subject to rotations about different axes will allow testing the plausibility of insect wings' inertial sensing capacity. Indeed, such a comparison of the forces acting on the halteres of *Calliphora* allowed Nalbach to conclude that whereas the primary inertial force is two orders of magnitude larger than the Coriolis force, the Coriolis force is the only force acting on the haltere that would allow a fly to determine the axis and sign of a rotational maneuver or perturbation (Nalbach, 1993). Thus, our findings that wing campaniform sensilla mediate changes in body posture and dynamics due to small disturbances in wing bending are very much in keeping with previous work on halteres.

In addition to the question of the relative strength of wing Coriolis forces during rotations, it remains unclear if insect neural systems can disambiguate between the detection of these different sources of wing bending. Campaniform sensilla arrangement varies dramatically between insects (Cole and Palka, 1982; Dombrowski, 1991; Gettrup, 1966; Schäffner and Koch, 1987a; Schmidt and Smith, 1985; Zacwilichowski, 1931), and the arrangement of campaniform sensilla on the wing could reflect a bias during evolution toward the detection of aerodynamic, Coriolis, or other forces relevant to behavior (Schäffner and Koch, 1987a; Schäffner and Koch, 1987b). Linking the spatial arrangement of campaniform sensilla to the encoding properties of the innervating neurons, as well as the wings' biomechanics, is crucial to the development of a full model of the wing's sensory role. Nevertheless, the results from our behavioral experiments suggest that wings themselves can indeed function not only as actuators during flight but also sensors to control body dynamics.

Much of the interest in halteres stems from their distinction as the only true gyroscopes in the animal kingdom, and this unique sensory function is unlikely to have evolved *de novo* in halteres

(Pix *et al.*, 1993; Pringle, 1948). Given that the halteres are evolutionarily derived from wings (hindwings in Diptera and forewings in Strepsiptera) and campaniform sensilla are found on both halteres and wings, behavioral reflexes mediated by aerodynamic or gyroscopic sensing might have evolved within wings and later been refined with the evolution of the halteres. Our results show that the wings of *Manduca* provide sensory information that can be used to control body posture, and thus dynamics, during flight. Thus, insect wings may indeed serve as both sensors and actuators during flight. Future work examining the forces to which the wing and wing campaniform sensilla are most sensitive during rotations, along with how this information is combined with other sensory modalities, will allow a more comprehensive understanding of the wings' role in flight as a dual sensor and actuator.

2.5 ACKNOWLEDGEMENTS

We thank M. Dickinson, R. Huey, T. Lindsay, E. Roth, P. Weir, and members of the Daniel lab for comments on this manuscript. Y. Munk helped program the motor used in the wing perturbation experiments. We thank W.P. Chan for his help obtaining SEM images.

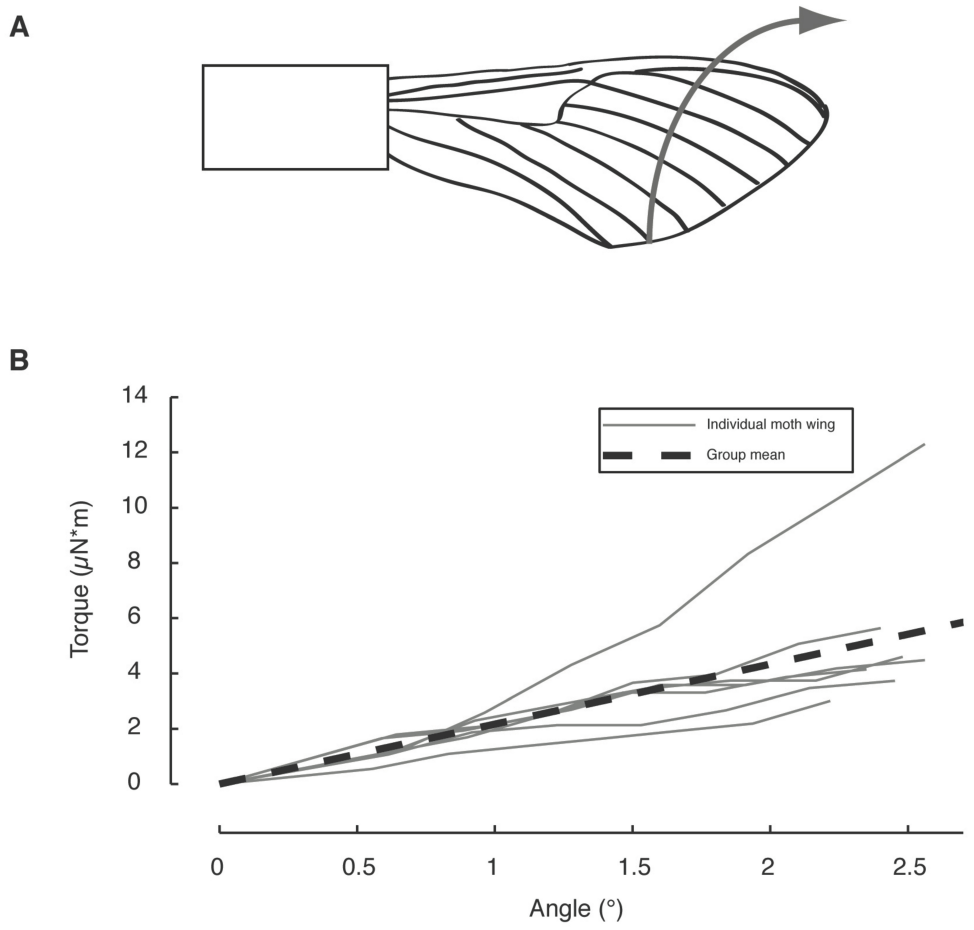

Figure 2.1 Measuring torsional stiffness. A) Wings were clamped in a micromanipulator and subject to a torque applied at the first cubital vein (grey arrow) by an insect pin placed on a scale by lowering the wing in 100 or 200 μm increments (See Materials and methods). B) Torsional stiffnesses of seven male *Manduca* wings (grey lines) and the group average (black dashed line).

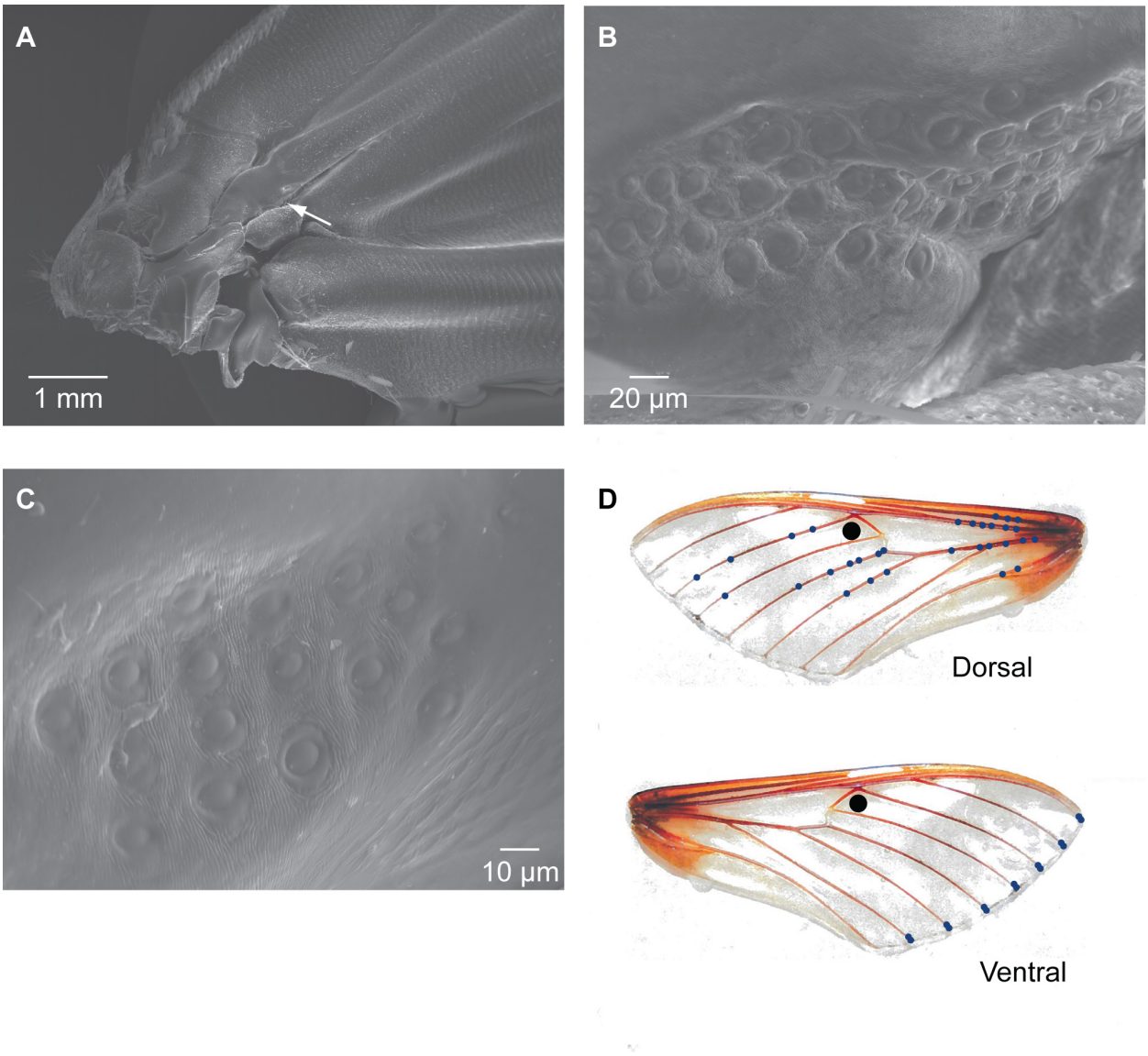

Figure 2.2 The forewings of *Manduca sexta* contain campaniform sensilla. (A) Patches of campaniform sensilla are found on the dorsal surface of the radius near the wing hinge. (B) SEM from a different wing (location as indicated in *a*) shows that each group is densely packed with campaniform sensilla. C) Ventral patches are arrayed in precise patterns, but are less dense than those on the dorsal surface. D) Locations of distal campaniform sensilla on the dorsal and ventral surfaces of a male forewing (blue circles). Black circles indicate the position of the magnets during wing perturbation experiments. The *Manduca* forewing is approximately 5 cm long.

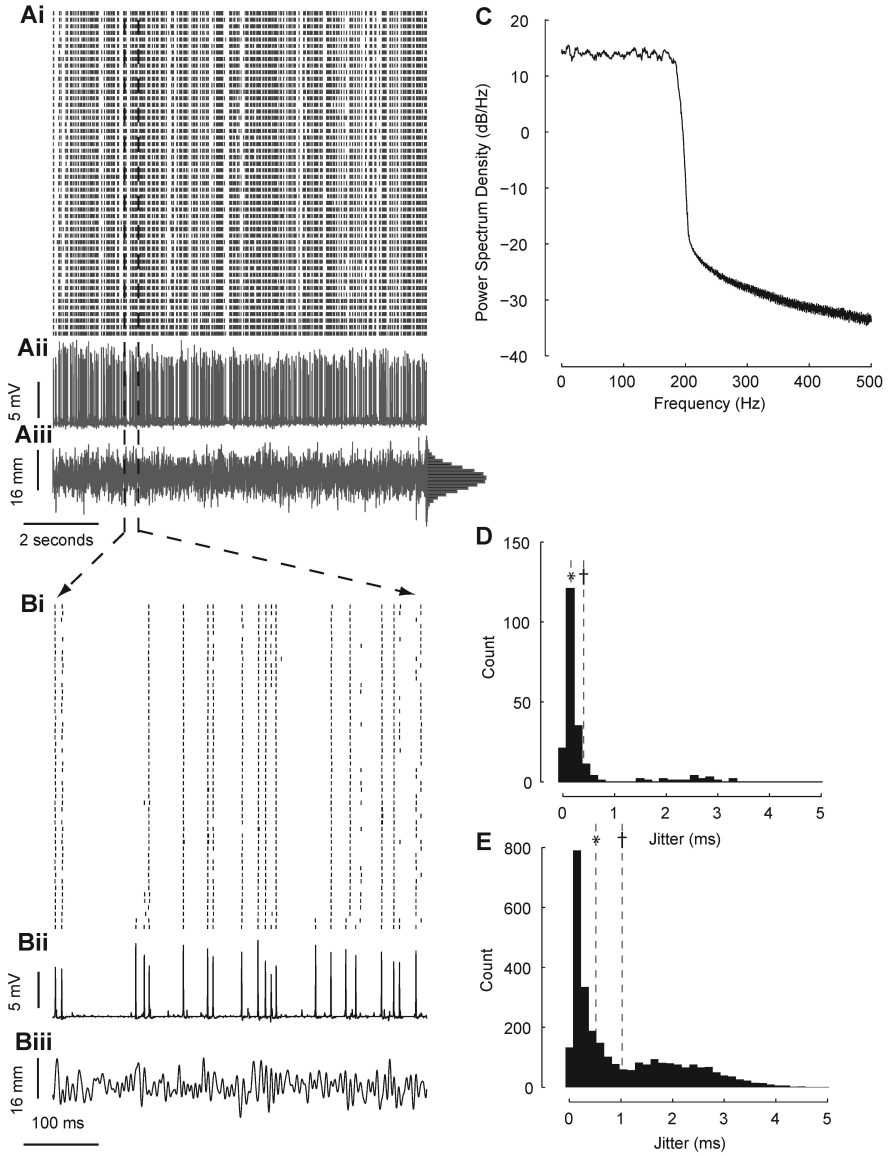

Figure 2.3 Temporal precision of campaniform sensilla afferent neurons. (Ai) Raster plot showing timing of spikes in response to repeated presentations of a 10 second Gaussian mechanical stimulus applied to the wing tip. (Aii) Intracellular voltage recorded from neuron during first stimulus presentation. (Aiii) Stimulus waveform, with histogram of amplitude distributions at right. (Bi-Biii) expanded 500 ms view of data in A. (C) Power spectra of stimulus, showing band limit of 10-200 Hz. (D) Histogram of jitter for 213 spiking events from same neuron as shown in A. Median jitter value: 0.16 ms (*), mean value ± 1 s.d.: 0.40 ± 0.70 ms (†). (E) Histogram of jitter for 2886 spiking events from 15 neurons in 7 animals. Median jitter value: 0.52 ms (*), mean value ± 1 s.d.: 1.02 ± 1.04 ms (†).

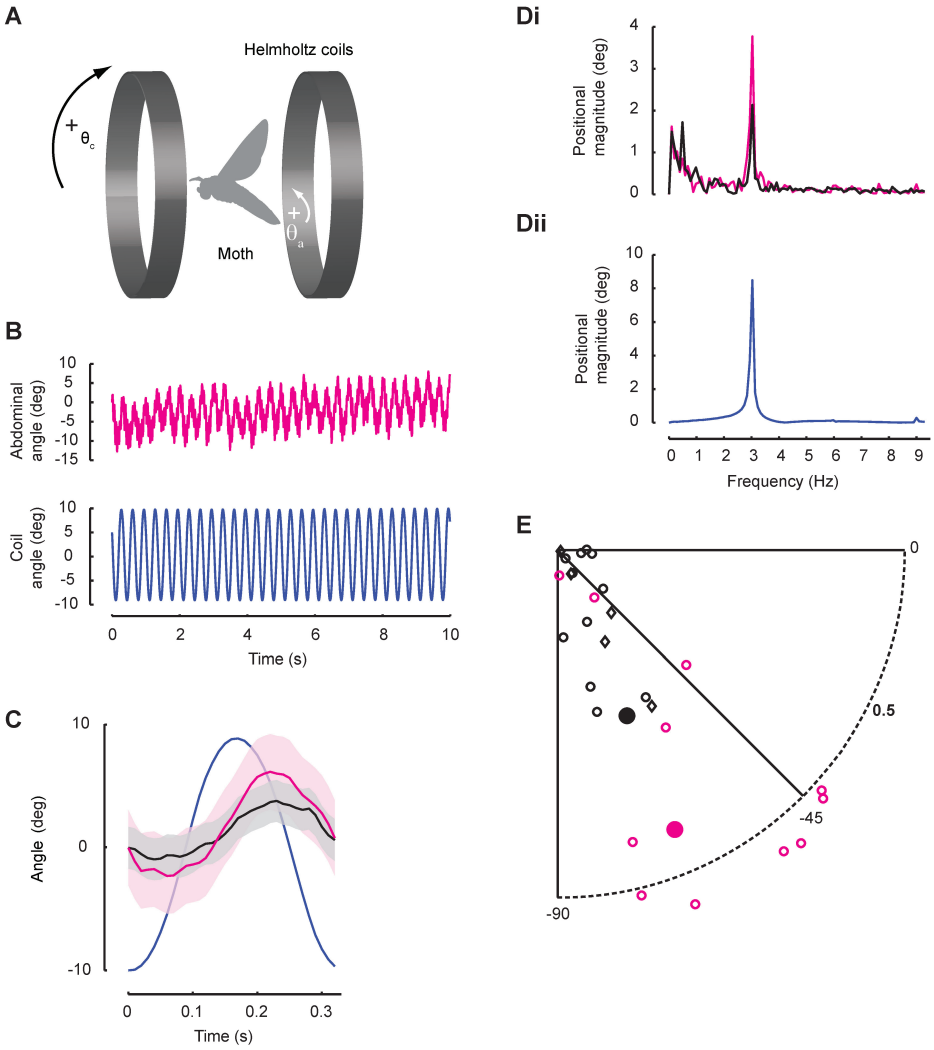

Figure 2.4 Moths respond to visual motion of Helmholtz coils in the absence of a magnetic field, whereas magnetic perturbation of the wings results in large abdominal responses. (A) Each moth was ventrally tethered at the thorax and placed between a pair of Helmholtz coils mounted to a stepper motor. Motion of the coils relative to the page is clockwise/counterclockwise. Figure is not to scale. (B) Example response (top, magenta) and stimulus (bottom, blue) during perturbation of the wingstroke. (C) Cycle averages of θ_c (blue line) and θ_a in response to the visual signal of the rotating Helmholtz coils (black) and in response to perturbation of the wingstroke (magenta, same trial shown in B). Shaded: ± s.d. This moth had magnets on its wings in both trials. (Di) Discrete Fourier Transform (DFT) of the abdominal responses in both

conditions shows a peak at the stimulus frequency, showing a gain of 0.258 and a phase of −67.0° in response to visual stimulation only (black), and a gain of 0.444 and a phase of −64.7° in response to visual and mechanical stimulation (magenta). Note that the signal shown in Figure 2.4B is non-stationary, which manifests as a large mean offset in the DFT. (Dii) DFT of the motion of the Helmholtz coils. (E) Polar plot of the gains and phases of abdominal responses. Distance from the origin indicates the gain of the response, and the angle indicates phase. Black circles: moths with magnets on their wings, subject to rotating Helmholtz coils (no magnetic field present; N = 17 trials, 4 moths). Black diamonds: moths subject to a rotating magnetic field without magnets on their wings (N = 5 trials, 3 moths). Magenta circles: moths with magnets on their wings subject to a rotating magnetic field (N = 12 trials, 4 moths). Solid circles indicate trials shown in Figure 2.4C. Moths subject to wing perturbations exhibit significantly greater mean abdominal response gain than moths with magnets on their wings, but no magnetic field ($P < 0.05$; repeated measures ANOVA).

Chapter 3. A NEW TWIST ON GYROSCOPIC SENSING: BODY ROTATIONS LEAD TO TORSION IN FLAPPING, FLEXING INSECT WINGS

Annika L. Eberle, Bradley H. Dickerson, Per G. Reinhall and Thomas L. Daniel
Journal of the Royal Society Interface 12: 20141088 doi: 10.1098/rsif.2014.1088

Insects perform fast rotational maneuvers during flight. While two insect orders use flapping halteres (specialized organs evolved from wings) to detect body dynamics, it is unknown how other insects detect rotational motions. Like halteres, insect wings experience gyroscopic forces when they are flapped and rotated and recent evidence suggests that wings might indeed mediate reflexes to body rotations. But, can gyroscopic forces be detected using only changes in the structural dynamics of a flapping, flexing insect wing? We built computational and robotic models to rotate a flapping wing about an axis orthogonal to flapping. We recorded high-speed video of the model wing, which had a flexural stiffness similar to the wing of the *Manduca sexta* hawkmoth, while flapping it at the wingbeat frequency of *Manduca* (25 Hz). We compared the 3D structural dynamics of the wing with and without a 3 Hz, 10 degree, rotation about the yaw axis. Our computational model revealed that body rotation induces a new dynamic mode: torsion. We verified our result by measuring wing tip displacement, shear strain, and normal strain of the robotic wing. The strains we observed could stimulate an insect's mechanoreceptors and trigger reflexive responses to body rotations.

3.1 INTRODUCTION

Insects acquire multimodal sensory information to control rapid flight maneuvers as they navigate through spatially and temporally complex natural environments. While both vision and

mechanoreception play important roles, these sensory modalities operate over very different time scales. Indeed, signal transduction mechanisms used by the visual system result in information processing speeds that are too slow to account for the rapid maneuvers these animals display in free flight (Land and Collett, 1974; Theobald et al., 2010). Thus, the timing precision, sensitivity and low latencies associated with mechanoreceptors make them critical features of insects' flight control circuitry.

Flies, for example, possess mechanosensory organs known as halteres that allow these animals to detect and correct for any perturbations to their flight path (Figure 3.1A–C). These small club-shaped structures sit behind the forewings and oscillate at wingbeat frequency (Fig. 3.1B). During rotational maneuvers, halteres experience a Coriolis force, which is proportional to the angular velocity of the body and is oriented orthogonal to the haltere's plane of oscillation (Nalbach, 1993; Pringle, 1948). This force is thought to drive small, out-of-plane movements of the haltere (Thompson et al., 2008), which would result in a normal strain at the haltere's base. While these movements have been demonstrated theoretically (Thompson et al., 2008), they have not been confirmed experimentally. However, Coriolis-induced haltere bending has been shown to excite embedded mechanoreceptors known as campaniform sensilla (Fig. 3.1C) (Fraenkel and Pringle, 1938; Hengstenberg, 1988; Pringle, 1948), triggering a host of compensatory reflexes (Dickinson, 1999; Fayyazuddin and Dickinson, 1996; Hengstenberg, 1988; Nalbach and Hengstenberg, 1994; Sherman and Dickinson, 2003). Interestingly, in engineering, an analogous method of strain sensing is commonly used in vibrating structural gyroscopes (Bhadbhade et al., 2008; Funk et al., 1999; Kagawa et al., 1996; Smith et al., 2012; Voss et al., 1997; Wu et al., 2002) where a mass attached to a beam is actuated via in-plane bending.

The evolution of the haltere has provided flies with the capacity to monitor inertial forces separate from the aerodynamic forces produced by the wings. However, only two insect orders, Diptera and Strepsiptera, possess such structures (Pix et al., 1993). The vast majority of insects instead possess the antecedent structures of halteres: an additional pair of wings. Thus, how most flying insects collect information about their body dynamics through mechanosensory structures is a long-standing problem in insect flight control. Although recent evidence suggests that the antennae of the hawkmoth *Manduca sexta* detect Coriolis forces and aid the animal in maintaining flight stability (Hinterwirth and Daniel, 2010; Hinterwirth et al., 2012; Sane et al., 2007), the use of antennae as putative inertial sensors does not preclude other structures from serving a similar role.

Since halteres are evolutionarily derived from wings, the wings of all insects might be capable of providing information about body rotations. Indeed, recent electrophysiological and behavioral evidence suggests that the campaniform sensilla embedded in the forewings of *Manduca* (Fig. 3.1D–F) provide the animal with input that mediates reflexes to virtual body rotations via wing bending (Dickerson et al., 2014). However, the structural dynamics of flapping wings during whole-body rotations, and how these dynamics affect campaniform sensilla to trigger these reflexes, are unknown at this time.

Furthermore, the dynamics of wing deformations during body rotations are likely substantially different from those of halteres under similar conditions: the mass distribution, flexural stiffness, and aerodynamic loading of wings are very different than halteres. The flexibility of insect wings, for example, depends strongly on their morphology (Chen et al., 2008; Combes and Daniel, 2003b; Combes and Daniel, 2003a; Ennos, 1988a; Ennos, 1988b; Ennos and Wootton, 1989; Norris et al., 2010; Walker et al., 2009; Wootton, 1981b; Wootton, 1992;

Wootton, 1993). There is also growing evidence that this flexibility enhances aerodynamic performance (Eberle et al., 2014; Heathcote and Gursul, 2007; Kang and Shyy, 2013; Mountcastle and Daniel, 2010; Nakata and Liu, 2012; Vanella et al., 2009; Young et al., 2009). However, flapping wings experience more than just the large aerodynamic and inertial forces associated with their flapping. Just as with halteres, they also experience additional inertial forces, specifically gyroscopic forces, as they undergo rapid rotational accelerations of their bodies. Thus, wing compliance may serve to improve more than just aerodynamic performance; wing compliance may also amplify the wings' ability to serve as a sensor of the body's angular velocity.

While the dynamics of structures undergoing concurrent actuation and rotation are well studied in engineered systems, particularly with regard to the blades of helicopters and wind turbines (Friedmann, 2004; Kaya and Ozdemir Ozgumus, 2007; Thakkar and Ganguli, 2004; Veers et al., 1998), these analyses often focus only on two bending axes and provide limited insight into the relationship between Coriolis forces and torsion. In addition, little work has been done to explore the dynamics that emerge in a highly flexible cantilever plate that is subject to concurrent rotation and orthogonal actuation, as in the case of an insect wing (Jankauski and Shen, 2014).

Here we explore how gyroscopic forces change the dynamics of a flapping, flexing wing. We sought to answer two questions. First, instead of undergoing small, out-of-plane deformations during rotations as are suggested for halteres, might flexible wings respond with a different dynamic mode? If so, is it then possible, using only the structural dynamics of a flapping, flexing wing, to determine the angular velocity of a whole-body rotation? To address these questions, we developed a computational model of a flapping, flexing plate subject to

whole-body rotations. We then experimentally validated these results with two different robotic flapping actuators subject to rotations about an orthogonal axis. We found that a flapping, flexing plate subject to rotation in an orthogonal axis exhibits significant torsion, a deformation mode not previously suggested for gyroscopic sensing in animals. Thus, we propose that existing strain sensory systems in the wings of flying insects could be used to provide gyroscopic information. In this way, the wings would serve a function similar to the halteres, long heralded as an exemplar of gyroscopic sensing in nature.

3.2 MATERIALS AND METHODS

3.2.1 *Computational model of insect wing structural dynamics*

We used Lagrange's equations in combination with a simple model of a deformable plate to derive the equations of motion for a flexible insect wing undergoing flapping motions in a rotating reference frame. This approach draws from the Rayleigh method (Rayleigh, 1877) and uses energy techniques rather than the force balance procedures that have been used previously (Pringle, 1948; Nalbach, 1993; Thompson, 2008).

We modeled the wing as a thin plate of uniform thickness, stiffness, and density (Fig. 3.2). Using *Manduca* wings as a guide for dimensions, the chord and span were set to 25 mm and 50 mm, respectively. The plate consisted of four nodes, each having three local degrees of freedom: two angular degrees of freedom about the local x- and y-axes, $f_i(t)$ and $q_i(t)$ respectively, and one displacement degree of freedom along the local z-axis, $d_i(t)$. To be consistent with our experimental setup, the positions and angles of the two nodes at the base of the wing (nodes 1 and 2 in Fig. 3.2) were prescribed as follows

$$\phi_1(t) = \phi_2(t) = \Phi(t) = A_{flap}\left[\sin(2\pi f_{flap}t) + 0.2\sin(4\pi f_{flap}t)\right] \quad 1a$$

$$\theta_1(t) = \theta_2(t) = 0 \tag{1b}$$

$$\delta_1(t) = \delta_2(t) = 0 \tag{1c}$$

where A_{flap} is the amplitude of flapping, f_{flap} is the wingbeat frequency and t is time. We did not allow any of the nodes to move in the local x- and y-directions (*i.e.* no stretching of the wing), but we did allow for displacement in the global X-, Y-, and Z-directions.

With the two nodes at base of the wing constrained, our wing model had six degrees of freedom remaining at nodes 3 and 4 (see Fig. 3.2). Thus, a vector, $\bar{q}(t)$, of the generalized coordinates is given by

$$\bar{q}(t) = \begin{bmatrix} \delta_3 & \phi_3 & \theta_3 & \delta_4 & \phi_4 & \theta_4 \end{bmatrix} \tag{2}$$

where d_i is the linear displacement of the i^{th} node along the z-axis, f_i is the angular displacement of the i^{th} node about the x-axis, and q_i is the angular displacements of the i^{th} node about the y-axis.

We assumed that the displacement of the plate could be described by

$$w(x,y,t) = \left[\bar{N}(x,y)\right]^T \bar{q}(t) \tag{3}$$

where $\bar{q}(t)$ is the vector of generalized displacements given by Eq. 2 and $\bar{N}(x,y)$ is a vector of shape functions that satisfy the boundary conditions (Reddy, 2004). For our model, we chose shape functions derived from fourth-order polynomials (Melosh, 1963). Although this model has

a limited ability to capture the higher modes of vibration, our goal was not to explore all that is physically possible. We chose this reduced order model as a more computationally efficient, but yet sufficiently accurate, approach to explore the underlying dynamics that develop when a wing is flapped and also rotated. Moreover, the results generated by this computational model agree quite well with those measured experimentally (see Results).

The position of all points, *m*, on the plate's surface in the plate's reference frame, *A,* is therefore given by

$$ {}^{A}\vec{r}^{\,m}(x,y,t) = \begin{bmatrix} x & y & w(x,y,t) \end{bmatrix}^{T} \qquad 4 $$

where *x* and *y* describe the position of each point in space, *t* is time, and *w*(*x,y,t*) is given by Eq. 3. For simplicity, we only allowed the flapping wing to rotate globally about the root of the support edge (*i.e.* body rotation with zero translation). Due to our simplified dynamics, the angular velocity, $\vec{\Omega}$, of the wing's reference frame, *A,* in the inertial frame, *S*, was therefore

$$ {}^{S}\vec{\Omega}^{A} = \begin{bmatrix} \dfrac{d\Phi}{dt} & 0 & \omega(t) \end{bmatrix}^{T} \qquad 5 $$

where *F* is the flapping rotation about the *X*-axis, which is prescribed at nodes 1 and 2 by Eq. 1a, and *w*(*t*) is the rotation of the body about the *Z*-axis.

In one set of simulations, we set the angular velocity of the body to be a constant value equal to the maximum angular yaw velocity of 800°/s encountered by *Manduca* during flight (Hedrick et al., 2009). However, since insects rarely perform maneuvers at constant angular velocities in

their natural environment, we also simulated a periodic angular velocity of the body. Thus, in the computational model, the angular velocity of the body was either described by

$$\omega(t) = \omega_c = 800^\circ / s \tag{6a}$$

or

$$\omega(t) = A_{rot} \sin(2\pi f_{rot} t) \tag{6b}$$

where f_{rot} is the frequency of the rotation and A_{rot} is the amplitude of the rotation. In the case of periodic rotation (Eq. 6b), the frequency and amplitude of the rotation were set to 3 Hz and 10°, respectively. We based the frequency of body rotation on previous experiments of *Manduca* subject to actual and simulated whole-body rotations (Dickerson et al., 2014; Hinterwirth and Daniel, 2010). The amplitude of the rotation was set by the amount of maximum rotation that we could achieve in our experimental setup (see next section).

With the position of all points on the plate surface given by Eq. 4 and the angular velocity of the wing in the inertial frame given by Eq. 5, we derived the equations of motion for a wing subjected to rotation using Lagrange's equations (see supplementary material). The general form of this system of equations is given by

$$\frac{d^2\bar{q}(t)}{dt^2} = M^{-1}M_a\frac{d^2\bar{x}_o}{dt^2} + \left(\frac{d\Phi}{dt}\right)^2 \bar{q}(t) - M^{-1}K\bar{q} + M^{-1}I_C{}^N\bar{\Omega}^A + M^{-1}\eta\frac{d\bar{q}(t)}{dt} \tag{7}$$

where $\bar{q}(t)$ is the vector of generalized coordinates (Eq. 2) for which we solved, M^{-1} is the inverse of the mass matrix, M_a is the applied acceleration mass matrix, $\bar{x}_o$ is a vector that describes the linear velocities of and angular velocities about basal nodes of the wing, K is the stiffness matrix due to strain energy of the plate, F is the prescribed input flapping given by Eq. 1a, I_c is an inertia-like matrix that describes the contribution of the Coriolis force for each

generalized coordinate, ${}^{N}\vec{\Omega}^{A}$ is the angular velocity vector of the wing in the inertial frame, and *h* is the damping factor. The terms on the right hand side correspond to the angular acceleration of the plate due to the initial conditions, the centrifugal force, the stiffness of the plate, the Coriolis force, and the wing damping, respectively.

We solved this system of second-order ordinary differential equations for the generalized coordinate vector $\bar{q}(t)$ over ten rotation cycles, starting from rest, using a fourth-order Runge Kutta method in MATLAB (The MathWorks, Natick, MA, USA). Simulations were run under five different conditions: flapping alone, constant rotation alone, periodic rotation alone, a combination of both flapping and constant rotation, and a combination of both flapping an periodic rotation.

We reported our results from the computational model using the position of the wing's tips and strain near the wing's base. The right and left wing tip positions (D_R and D_L, respectively) are given by

$$D_R = \begin{bmatrix} -a & 2b & w(-a,2b,t) \end{bmatrix}^T \tag{8a}$$

$$D_L = \begin{bmatrix} a & 2b & w(a,2b,t) \end{bmatrix}^T \tag{8b}$$

where *a* is half of the chord length, *b* is half of the span length, and *w(x,y,t)* is the deformation found above. In addition, the strain is given by

$$\vec{\varepsilon}(x,y,t) = -\frac{h}{2}\begin{bmatrix} \frac{\partial w(x,y,t)}{\partial x^2} & \frac{\partial w(x,y,t)}{\partial y^2} & 2\frac{\partial w(x,y,t)}{\partial x \partial y} \end{bmatrix}^T \tag{9a}$$

$$\vec{\varepsilon}(x,y,t) = -\frac{h}{2}\begin{bmatrix} \varepsilon_{xx}(x,y,t) & \varepsilon_{yy}(x,y,t) & \varepsilon_{xy}(x,y,t) \end{bmatrix}^T \tag{9b}$$

where h is the thickness of the wing, $\varepsilon_{xx}(x,y,t)$ is normal strain in the x-direction, $\varepsilon_{yy}(x,y,t)$ is normal strain in the y-direction, and $\varepsilon_{xy}(x,y,t)$ is shear strain in the x-y plane.

3.2.2 *Robotically actuated model with position tracking*

To validate the results of our computational model we built a robotic actuator to oscillate a model insect wing in a flapping motion while also rotating it about an orthogonal axis (Fig. 3.3). This experimental setup was used to measure the displacement of the tips of a model wing actuated in air.

By optically tracking the position of the wing, we measured the dynamics of wing deformation during a combination of flapping and body rotation. Our model wing consisted of a 50 mm by 25 mm acrylic sheet with a flexural stiffness of 10^{-5} Nm^2 that well approximated a *Manduca* forewing (Combes and Daniel, 2003b). To track bending during each trial, we drew a 5 by 9 grid of fiduciary markers on our wing model with correction fluid (Fig. 3.3B). The model wing was attached to the shaft of a servomotor controlled by a length driver (Model 305B Dual-Mode Lever Arm System, Aurora Scientific Inc., Aurora, ON, Canada) and the frequency and amplitude of the flapping oscillation were controlled with a function generator (3311A Function Generator, Hewlett-Packard, Palo Alto, CA). The oscillation amplitude (15°) was constrained by the motor power and was lower than that of *Manduca*. However, the wing was flapped at the typical *Manduca* wingbeat frequency of 25 Hz.

We secured the robotic actuator onto a rigid aluminum frame that was mounted to a stepper motor (Hinterwirth and Daniel, 2010). To be consistent with our computational model, the rotation of this motor was controlled using a custom Arduino script that generated a 10°, 3 Hz

sinusoid about the z-axis via a micro-step controller (G201, GeckoDrive Inc., Tustin, CA). We mounted a high-speed camera (Phantom Miro, Vision Research, NJ, USA) to the frame and recorded at 500 frames s^{-1}, with a 400μs shutter speed. An orthogonal view of the wing was provided by a mirror attached to the frame above the model wing in the view of the camera.

We measured wing tip motions under the following conditions: flapping alone, rotation alone, and flapping and rotation. All trials were conducted for 10 seconds to allow the system to reach steady state motion. We digitized the videos using a custom MATLAB script (The MathWorks, Natick, MA, USA), tracking six points on the model wing: the free ends of the top and bottom of the wing, and the two corners at the base of the wing. To be consistent with the results from our computational model, these values were reported using the variables D_R for the right wing tip and D_L for the left wing tip (see Eq. 8a,b).

3.2.3 *Robotically actuated model with strain measurement*

A second experimental system allowed us to measure model wing strain during a combination of flapping and rotation about the *z*-axis. The model wing consisted of a piece of 50 mm by 25 mm acrylic with a thickness of 127 μm. To measure shear strain, we glued a 350 Ω rosette strain gauge (SGD-2/350-RY53, Omega Engineering Inc., Stamford, CT, USA) to the wing at about 1/4 of the span along the mid-chord (Fig. 3.3C). The rosette was placed such that two of the strain gauges in the rosette were aligned at 45 degrees to the span with the remaining gauge coincident with the mid-chord. Since our primary interest was to detect shear strain caused by torsion, recordings were only taken from the two strain gauges oriented at 45 degrees to the span. For the measurement of normal strain, we glued two 350 Ω linear strain gauges (KFH-3/350-C1, Omega Engineering Inc., Stamford, CT, USA) onto either edge of the chord at the

base of a separate model wing (Fig. 3.3D). In all cases, the strain gauges were connected in separate quarter-bridge configurations so that we could measure the strain of each gauge independently.

The model wing was attached onto a camshaft setup designed to produce sinusoidal motion (25 Hz, 15°) using the previously mentioned function generator. As in the prior experimental setup, the system was actuated in air with periodic (3 Hz, 10°) rotation about the z-axis. We measured wing strain under the same conditions as the prior setup: flapping alone, rotation alone, and flapping and rotation. Signals from the strain gauges were amplified 100x (Transbridge 4M, WPI, Sarasota, FL, USA) and sampled at 5 kHz (USB-6008, National Instruments, Austin, TX, USA).

3.3 RESULTS

Below we summarize computational results for flapping wings subject to constant yaw rotation as well as periodic yaw (z) rotations. The latter are compared to experimental results for flapping wings subject to periodic yaw rotations.

3.3.1 *Torsional deformation emerges from a combination of flapping and constant yaw rotation in the computational model*

Simulations from the computational model revealed that wings subject to both flapping (25 Hz, 20°) and constant yaw rotation (w_c = 800°/s) exhibit torsional deformations (Fig. 4). These results are seen in the temporal pattern of tip displacements (D_R and D_L). The difference between these displacements (*i.e.* the relative tip displacement, $D_L - D_R$) (Fig. 3.4C) is about 100 times

smaller than the absolute tip displacement (Fig. 3.4A). Though small, this difference in the displacement of the two wing tips during concurrent flapping and rotation (solid line in Fig. 3.4C) is indicative of wing torsion. This phenomenon is not seen in either pure flapping or pure rotation (dashed line in Fig. 3.4C). Moreover, the double peaks in the sinusoidal pattern of deformation during flapping and rotation (dashed lines in Fig. 3.4C) occur at twice the flapping frequency and are therefore a signature of the Coriolis force. Indeed, when we reverse the direction of the angular velocity (*i.e.* w_c = -800°/s), the peaks that occur at twice the flapping frequency due to the Coriolis force also reverse sign (Fig. 3.4D).

To further explore the dynamics of Coriolis-induced wing torsion, we plotted the differences in wing deformation and strain with and without constant yaw rotation at several snapshots in time during a single period of flapping (Fig. 3.5). While the differences in normal strain in the span-wise (*y*) direction (Fig. 3.5C) and shear strain in the *x*-*y* plane (Fig. 3.5E) are of the same order of magnitude (0.001% strain), the difference in the normal strain along the chord-wise (*x*) direction (Fig. 3.5D) is about 100 times smaller. This difference in chord-wise normal strain is due to changes in span-wise lengthening generated by the tiny centrifugal forces produced by wing flapping combined with the Poisson effect: the model wing compresses in the chord-wise direction as it is stretched in the span-wise direction. As a result, the largest differences in chord-wise normal strains are near at the tip of the wing because that is where the span-wise lengthening is greatest.

Additionally, the difference in normal strain in the span-wise (*y*) direction displays peak regions that oscillate from side-to-side near the base of the wing. On the other hand, the difference in shear strain is largest in the center of the wing. These observations are consistent with theoretical results for a plate undergoing torsion (Reissner and Stein, 1951): maximum

shear strain occurs at the center of the plate and maximum normal strain along the span-wise direction occurs at the base of the plate. Thus, when the plate undergoes rotation while flapping, a new mode of deformation appears: torsion.

3.3.2 *Wing tip deformation reveals torsion in flapping wings subject to periodic yaw rotation in both computational and physical models*

As mentioned above, for both experimental convenience and biological relevance, we examined tip deformations in both computational and experimental wings subject to a combination of flapping and periodic yaw rotations. This approach provided a direct validation of our computational results. Since our robotic models were actuated in air, they also include aerodynamic loading and therefore allow us to examine the relative impact of aerodynamic forces. Since prior work showed that aerodynamic forces do not contribute substantially to wing bending at the scale of *Manduca* (Combes and Daniel, 2003a), we expected our experimental and computational results for wing torsion to be very similar.

Indeed, we observed strong similarities between the relative tip displacement (*i.e.* difference between the model wing's two free ends, *DD*) of our computational and experimental results (Fig. 3.6). When subject to flapping alone, the relative tip displacement is zero for the computational model (Fig. 3.6A). While the relative tip displacement during flapping alone is not exactly zero in the physical experiment, it is quite small (~5 μm) and rather noisy (Fig. 3.6D). In contrast, during the combination of flapping and rotating about an orthogonal axis, the relative tip displacement is much larger (~50 μm) and strongly periodic (Fig. 3.6E). This result holds true for both the computational (Fig. 3.6B) and robotic (Fig. 3.6E) models.

To determine the frequencies present in these periodic signals, we computed the fast Fourier transforms (FFTs) of the relative tip displacements and evaluated the difference between the amplitudes of the FFTs for flapping alone and flapping and rotating (see supplementary material for further explanation). Our results show strong peaks at the imposed flapping frequency of 25 Hz ± rotation frequency (3 Hz) for both our computational and physical models (Fig. 3.6C,F). This phenomenon, known as amplitude modulation, results from the Coriolis force, which is proportional to the angular velocity (a sine wave at rotation frequency) times the velocity of the wing (a cosine wave at wingbeat frequency). Using the product-to-sum trigonometric identity,

$$\sin(\alpha)\cos(\beta) = \frac{\sin(\alpha+\beta)+\sin(\alpha-\beta)}{2}. \qquad 10$$

Thus, the Coriolis force causes torsional oscillations at wingbeat frequency, modulated by the rotation frequency. Moreover, the magnitudes of these oscillations in relative tip displacement (Fig. 3.6C,F) are about three orders smaller than the absolute tip displacement (~30 mm).

3.3.3 *Torsion caused by rotational perturbations of flapping wings is reflected in wing strain*

The Coriolis-induced torsion that we observed via relative wing tip displacement is also reflected in the spatiotemporal patterns of shear and normal strain. For both flapping alone and flapping with imposed periodic body rotation, our computational and experimental results exhibit periodic shear (Fig. 3.7) and normal (Fig. 3.8) strain. Shear strain, as measured near the base of the wing at the mid-chord, is on the order of 0.01% strain. On the other hand, normal strain, as measured in the span-wise direction at either side of the wing base, is an order of magnitude

larger (0.2% strain). As expected, when the wing is subjected to body rotation alone, both shear and normal strain are zero (data not shown). In all cases, the experimental and computational models exhibit equivalent strain dynamics.

The difference between flapping with versus without body rotation for both shear and normal strain is difficult to discern looking at the two signals side by side (*e.g.* Figs. 3.7A,B and 3.8A,B). Since the experimental results for pure flapping versus combined flapping and rotating are not phase-matched, we cannot perform a simple subtraction. As such, we instead computed the FFTs of the strains under each condition and then computed the difference between the magnitudes of the FFTs. We performed this analysis separately for both shear and normal strain under the two conditions of flapping with and without body rotation (Figs. 3.7C,F and 3.8C,F). Similar to the displacement (Fig. 3.6), both shear and normal strain exhibit sharp peaks at the wingbeat frequency ± the rotation frequency and its first harmonic. The experimental results also have additional peaks at wingbeat frequency and its harmonics, which are likely due to our inability to exactly control the flapping frequency in the experiment (*e.g.* less than 1% difference in frequency causes the difference of the FFTs to have large peaks at the flapping frequency – see supplementary material).

Our computational results for periodic yaw (z) rotation also show spatiotemporal patterns of shear and normal strains on the surface of the wing that are similar to those noted above for constant rotation (Fig. 3.5). As for constant rotation, the maximum and minimum values of difference in the span-wise normal strains between flapping and rotating versus flapping alone oscillate near the base of the wing. Moreover, as during constant rotation, the maximum and minimum values of the difference in the shear strains between flapping with versus without periodic rotation are largest at the center of the wing. However, in the case of periodic rotation,

the magnitude of the strain varies at both the wingbeat frequency and the frequency of the yaw rotation.

3.4 Discussion

As flapping, flexing, and flight-force generating structures, insect wings are subject to a host of aerodynamic and inertial forces. These forces, in turn, interact with the wings' structural dynamics to generate complex spatial and temporal patterns of deformation. In this study, we undertook a series of computational and experimental approaches to investigate how such patterns of wing deformation depend upon body rotations. Our work was motivated, in part, by the notion that wings, as evolutionary antecedents of halteres, might themselves provide information about body dynamics. Additionally, biological systems might provide inspiration for new ways to generate gyroscopic sensory devices.

Our goal here is to reveal the principles that govern the structural dynamics of flapping insect wings during body rotations. As a result, we only considered simplified flapping kinematics and assumed a flexible plate of uniform stiffness and mass distribution. In actuality, insect wings are neither homogeneously stiff (Combes and Daniel, 2003c) nor do they have uniform mass distribution. Factoring in these characteristics may affect the torsional dynamics and change the strain distribution on wings. Regardless, we have uncovered a unique mechanism that easily enables the wings to detect information previously thought to require complex neural processing (Chan et al., 1998).

Here we found that flapping, flexible wings subject to rotations about an orthogonal axis reveal a pattern of torsional deformation not noted previously. In addition, wings exhibit periodic normal and shear strains that are a direct consequence of the Coriolis forces acting on them. During rotations, these changes in strain could stimulate embedded mechanoreceptors and trigger

correctional reflexes. In this way, insect wings would serve a role similar to halteres, the prototypical biological gyroscopes.

3.4.1 *Insect wings undergo torsion during body rotations, resulting in spatiotemporally varying strain*

Whereas a great deal of effort has gone into understanding the causes of wing bending, torsion in insect wings has received far less attention. Much of the focus in this regard pertains to measuring the torsional stiffness of insect wings (Wootton, 1993) or understanding the basis for torsion during hovering flight (Ennos, 1988b). Ennos (Ennos, 1988b), for example, concluded that torsion in hoverfly wings was due primarily to inertial forces. But inertial forces in a rotating reference frame arise from both rectilinear and rotational accelerations, one of which is the acceleration arising from the superposition of orthogonal rotational motions (the Coriolis acceleration). Thus, the inertial forces that result from body rotations could cause wing torsion and thereby convey information about rotation rate.

Our computational results reveal a complex spatiotemporal pattern of strain that arises when flapping wings are subject to rotation about an axis orthogonal to their flapping, as during a body rotation. Whether we simulate constant or periodic body rotation, three key results emerge. First, wings undergo a large bending deflection along the span driven by inertial bending moments produced by flapping. This result is consistent with prior studies highlighting the dominant role of inertial and elastic mechanisms underlying wing and haltere deformation (Combes and Daniel, 2003a; Daniel and Combes, 2002). Second, superimposed upon that large bending deformation is a smaller torsional deformation that is seen in the difference of the tip displacement at the corners of our rectangular wing. In contrast to the minuscule lateral deflections suggested for

halteres subject to Coriolis forces, the high lateral second moment of area of wings prohibits any such deformation and thus torsion emerges. Third, wing torsion appears as periodic patterns of shear and normal strains distributed over the wing surface. In contrast to normal strains, where the dominant signal arises from in-plane bending, shear strains directly measure torsion and are insensitive to the large in-plane bend.

3.4.2 *Changes in wing strain could stimulate mechanosensors, enabling insects to detect body rotation*

In halteres, the detection of Coriolis forces is thought to require extreme directional sensitivity of the campaniform sensilla in order to respond to exceedingly small lateral deflections in the presence of large in-plane bending moments that result from haltere flapping (Fraenkel and Pringle, 1938; Pringle, 1948). While such sensitivity has been suggested for haltere campaniform sensilla (Zill and Moran, 1981; Zill et al., 1981), wing campaniform sensilla are highly unlikely to experience lateral deflections analogous to those suggested for halteres. Perhaps alternate mechanisms, which combine our results with previous results on the neural timing precision of campaniform sensilla, suggest other ways to detect Coriolis forces.

One possible mechanism could involve detecting the temporal separation of peak strain as opposed to changes in strain magnitude. We show that the magnitudes of peak normal strains at the wing base are large and that the small differences that arise from Coriolis-induced torsion result in shifts in the timing of peak strain. As has been suggested for halteres (Fox et al., 2010), this spatiotemporal pattern of wing strain could be encoded by the nervous system using subtle shifts in the phase of firing of campaniform sensilla across the wing. While this encoding strategy would require a high level of temporal precision from wing campaniforms, high

temporal precision is a hallmark of campaniform sensilla on halteres (Chapman et al., 1973; Dickinson, 1990a; Dickinson, 1990b; Fox et al., 2010) and wings (Dickerson et al., 2014). In fact, the detection of the wing torsion dynamics that we observed is well within the encoding bandwidth limits of campaniform sensilla. Moreover, recent computational work suggests that the incorporation of neuronal filters, which capture aspects of a signal's time history, onto the strain field of a flapping flexing plate enhances the ability to detect body rotation (Brunton et al., 2014). Thus, rather than relying on magnitude alone, gyroscopic sensing may require an encoding strategy that includes both the spatial and temporal aspects of strain.

No matter how the strain sensing occurs, this unique sensory role through the process of actuation would make the wing both a sensor and an actuator. That is, by flapping for propulsion and maneuverability, the wing and its embedded campaniform sensilla could detect phenomena during perturbations or maneuvers that would be otherwise unavailable to the animal. This sensory role for the wings could predate their evolutionary modification into halteres, organs with a demonstrated capability for sensing angular velocity.

3.5 Conclusions

We propose that insects can detect the angular velocity of their body via changes in the structural dynamics of their wings. Through the development of computational and robotically actuated wing models, we show that torsion emerges when a flapping, flexing wing is subject to body rotations. This torsion leads to an increase in strain over the wing's surface, which could stimulate the campaniform sensilla embedded in the wing and thereby trigger compensatory reflexes. Thus, we demonstrated that there is indeed a unique structural dynamic mode that develops in the wing, which could inform an insect about its body dynamics.

These results have broad implications for our understanding of biological gyroscopes and for the design of engineered systems. For example, our results indicate that information about body dynamics could be determined by embedding strain gauges directly onto the surface of flexible airfoils already being actuated for propulsion or energy harvesting (*e.g.* micro air vehicles, turbine blades, and helicopter blades). Since the spatiotemporal pattern of strain has implications for optimal sensor placement, future work will examine the extent to which this information might allow us to 1) identify the biological placement of campaniforms on insect wings and 2) inform sensor design for engineered systems. Furthermore, our results suggest that the time has come for a re-examination of the haltere's structural dynamics. Future work will modify prior haltere models to allow for torsional deformation and test hypotheses regarding the importance of temporal encoding.

Through the exploration of biological gyroscopes we have uncovered principles that might be useful for engineering design. Conversely, our use of engineering analysis has provided insight into the form and function of the mechnanosensory structures embedded in insect wings.

3.6 ACKNOWLEDGEMENTS

BHD and ALE contributed equally to this work. The authors thank Bing Brunton, Eatai Roth, Brian Hinson, and the Daniel Lab for useful discussions and comments on this manuscript.

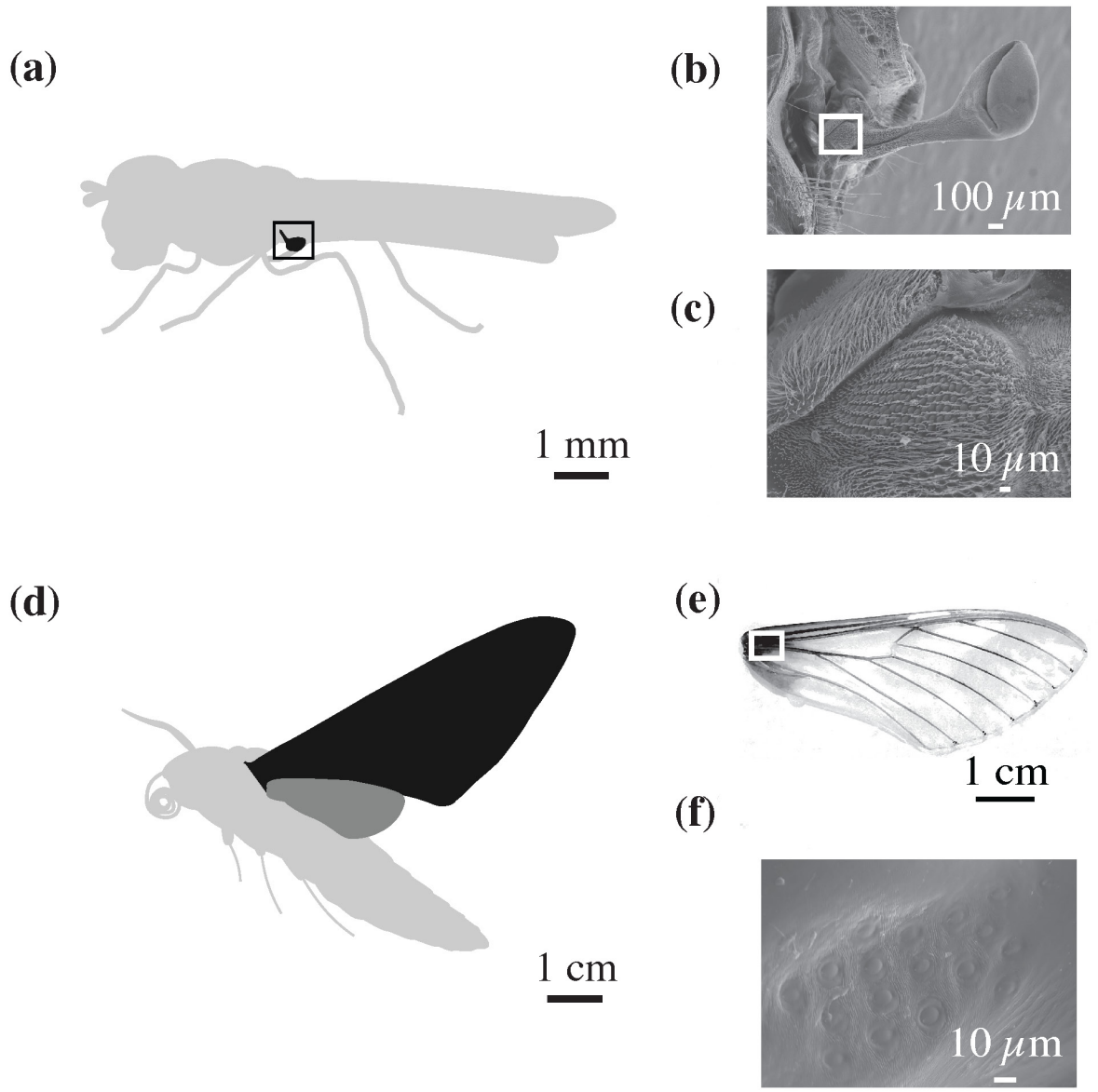

Figure 3.1 Insect halteres (A-C) and wings (D-F) possess campaniform sensilla. A single haltere on a robber fly is highlighted via the black box in (A) and magnified by SEM images in (B,C), where the white box in (B) indicates the location magnified in (C). The wing of a hawkmoth is highlighted in black in (D). A photograph of a cleared wing is shown in (E), where the white box in (E) shows the location the SEM image of campaniform sensilla in (F).

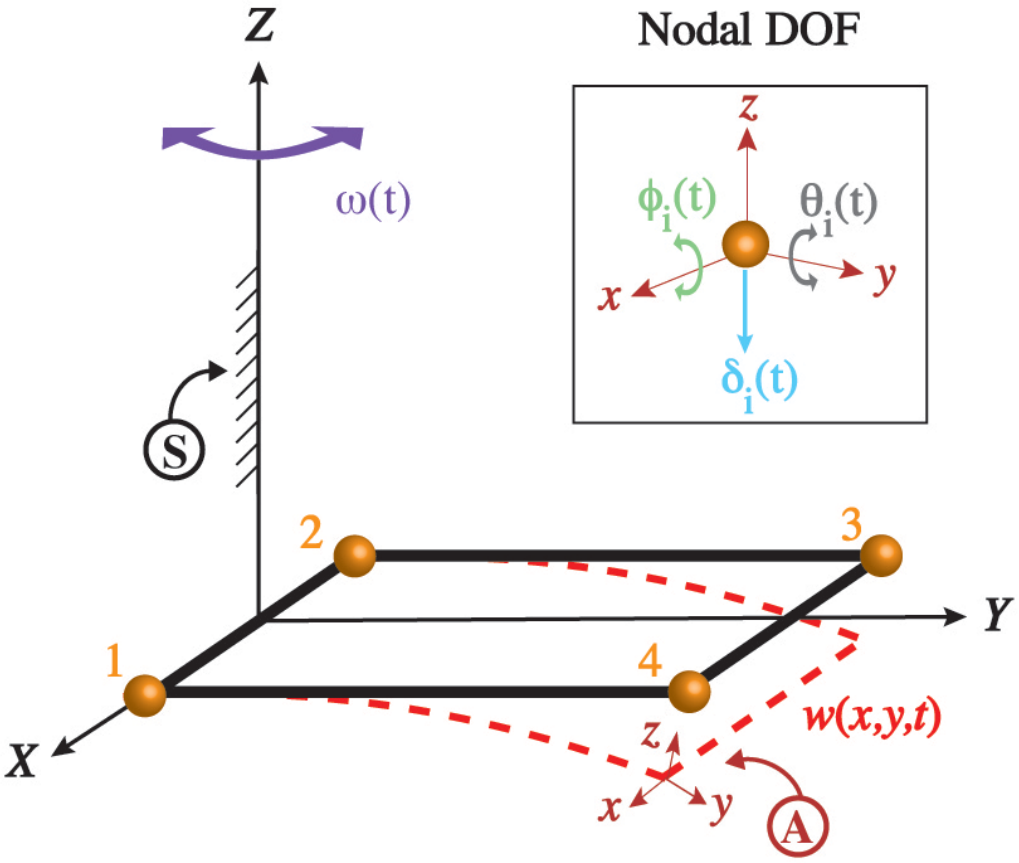

Figure 3.2 Diagram of the computational wing model, where symbols indicate the following: $w(x,y,t)$ is the z-displacement of the surface, which varies in space (x,y) over the surface of the wing and also in time, t; and $\omega(t)$ is the angular velocity of the body frame about the inertial Z-axis. The inertial frame, denoted by S, corresponds to the X, Y, and Z axes, and the local frame of the wing, denoted by A, is defined by the x, y, and z, axes. Orange spheres illustrate the nodes of the computational model. Nodes 1 and 2 are prescribed to move according to a single degree-of-freedom, which is a flapping input about the local x-axis. Nodes 3 and 4 are allowed three local degrees of freedom shown in inset: rotation about the local x-axis, $\phi_i(t)$, twist about the local y-axis, $q_i(t)$, and vertical displacement along the local z-axis, $\delta_i(t)$.

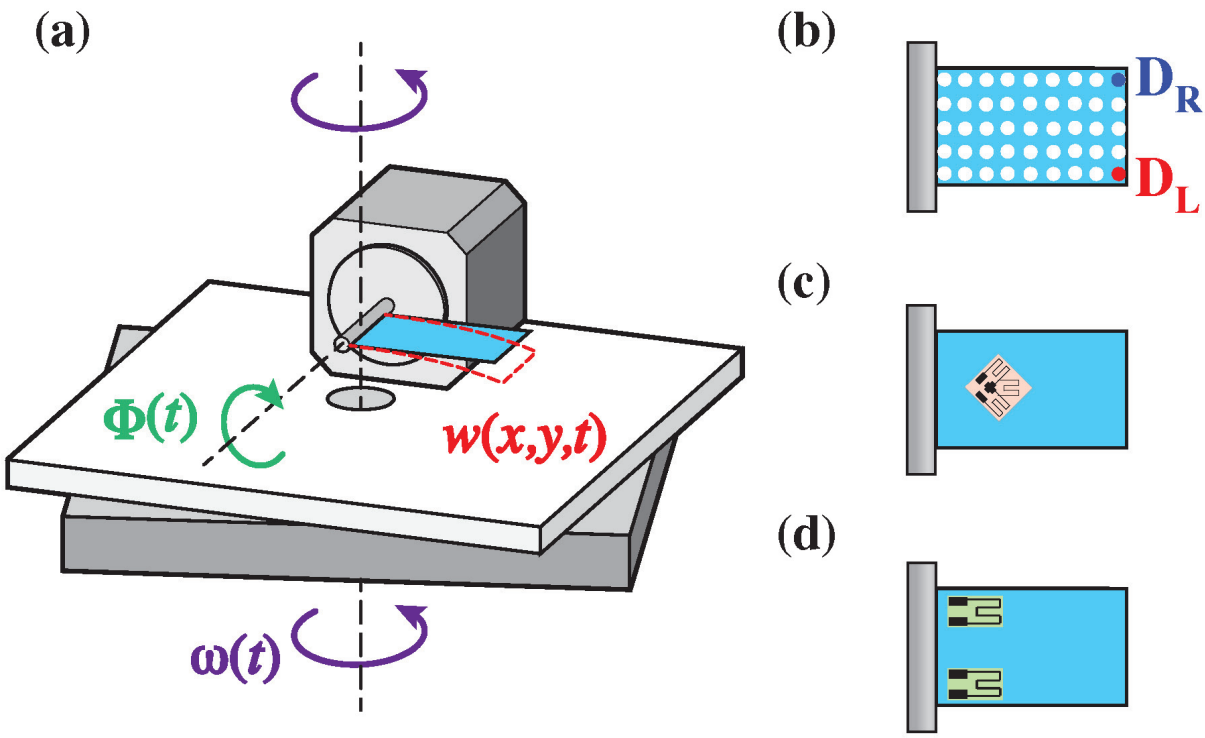

Figure 3.3 Diagram of the robotically actuated wing setup (A), where *F(t)* is the flapping input and *ω(t)* is the angular velocity input about the vertical. The model wing is viewed from the side and a trace of its displacement, *w(x,y,t),* (dashed red line) corresponds to *w(x,y,t)* in the computational model (Fig. 3.2). To measure displacement, the wing model was marked with correction fluid to create a 5 by 9 grid of fiduciary markers (B). To measure strain, strain gauges were adhered to the wing's surface. In the case of shear strain, a single rosette was placed at about ¼ span along the mid-chord (C). When evaluating normal strain, two linear strain gauges were applied to either side of the wing's base (D).

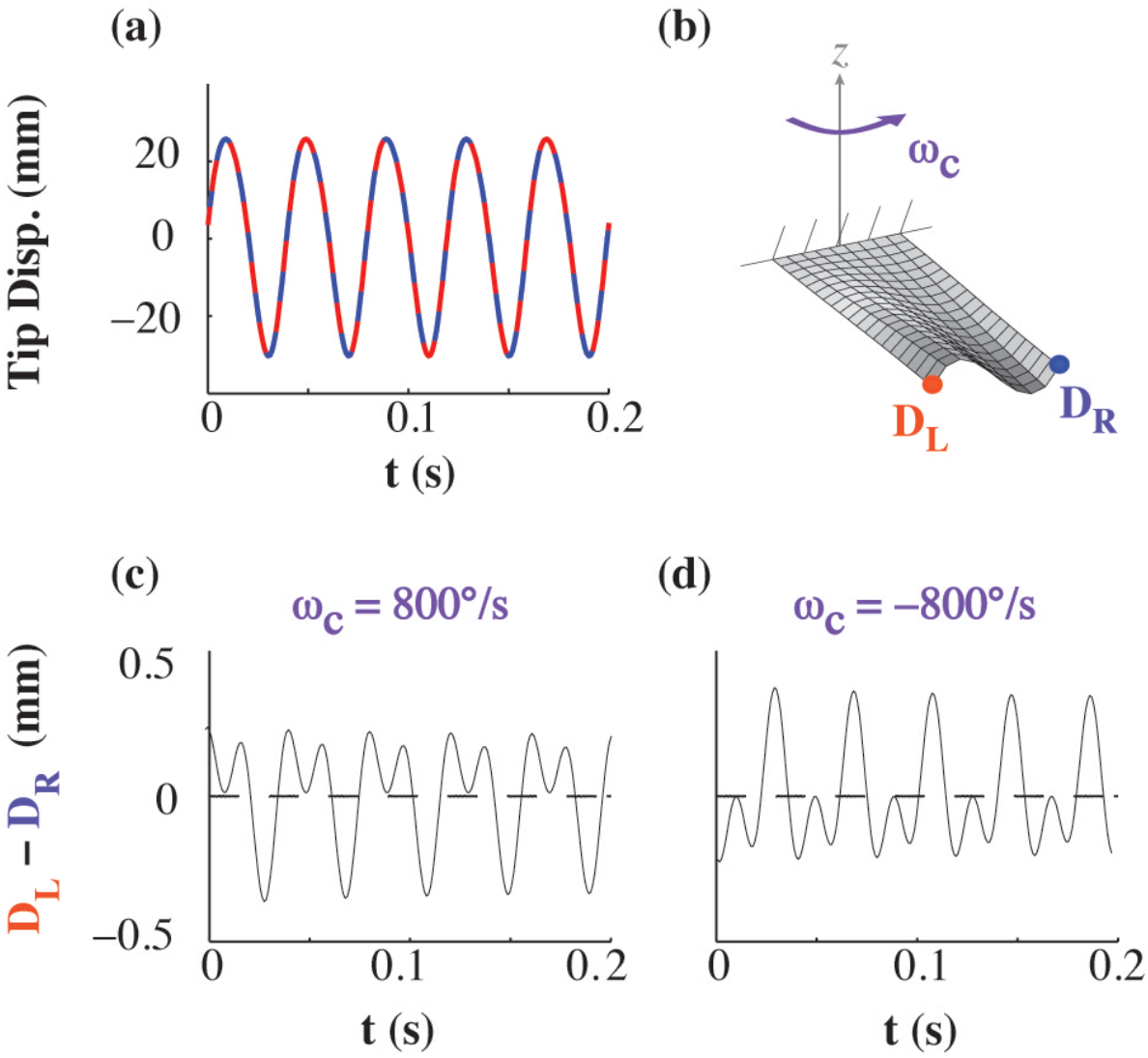

Figure 3.4 The displacements of the left (D_L, solid red) and right (D_R, dashed blue) wingtips of the computational wing model are very similar over time, t, for flapping alone (A). When the wing twists due to an applied constant rotation, ω_c, illustrated in (B), the difference between these two tip displacements changes. This difference is effectively zero when the wing is just flapping (dashed lines in (C) and (D)). However, when the wing is flapping while also rotating (solid lines in (C) and (D)), the difference in tip displacement oscillates at wingbeat frequency and twice wingbeat frequency. When the sign of the rotation is reversed, the signature at twice the wingbeat frequency (indicative of the Coriolis force) also reverses sign (D).

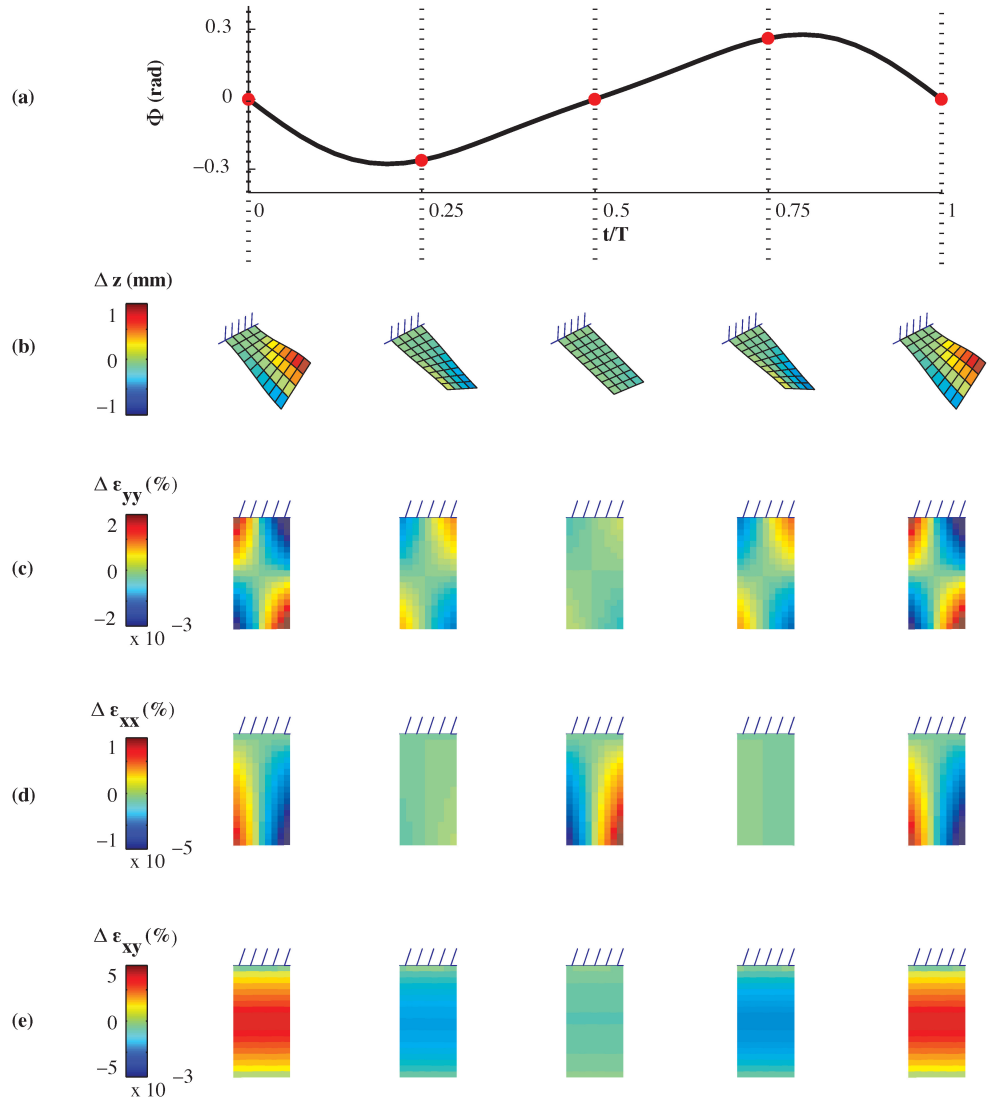

Figure 3.5 Torsion emerges in the computational model when the wing is flapped while it is also rotated at constant angular velocity of 800°/s. As shown in (A), the input flapping angle, *F*, varies over the relative time in the flapping cycle, *t/T*. The displacement of the model wing and the strain at its surface change in both space and time. At several snapshots in time (indicated by the filled circles and dotted vertical lines in (A)), spatial contours of the difference between flapping and rotating versus flapping alone are shown for four parameters: displacement, Δz (B); normal strain along the *y*-axis, $\Delta\varepsilon_{yy}$ (C); normal strain along the *x*-axis, $\Delta\varepsilon_{xx}$ (D); and shear strain in the *x*-*y* plane, $\Delta\varepsilon_{xy}$ (E). Coloring refers to the magnitude of each parameter as indicated by the color bars on the far left.

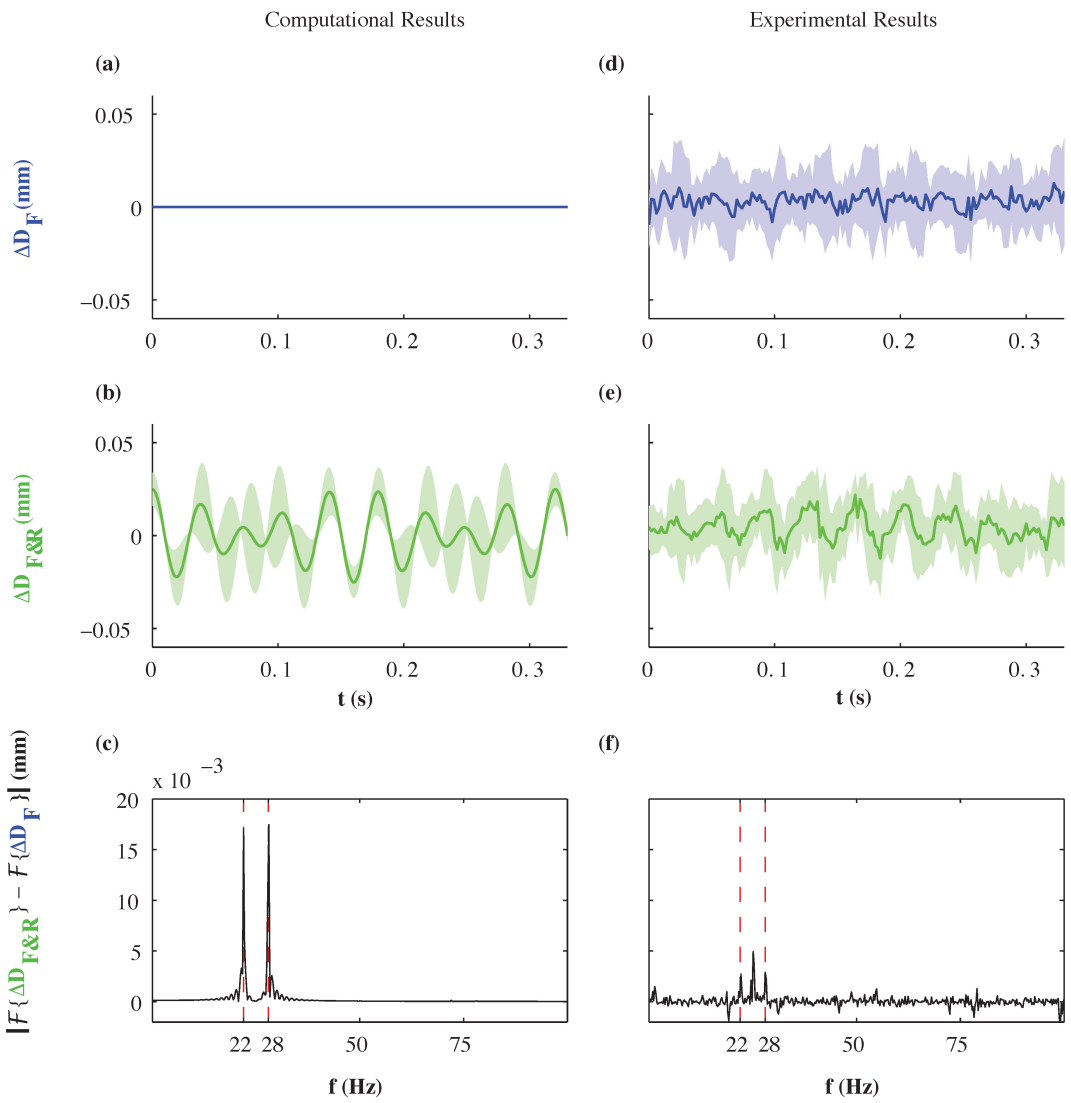

Figure 3.6 The difference between the displacement of the left (D_L) and right (D_R) endpoints of the wing, ΔD, versus time, t, for flapping alone (A,D) and flapping and rotating with periodic angular velocity (B,E). The subscripts of ΔD are F for flapping alone and $F\&R$ for flapping and rotating. Time domain results for a time-average taken over ten rotation cycles are shown for computational (A-B) and experimental (D-E) models. Shading denotes standard deviation. Frequency domain results of the difference in amplitude of the fast Fourier transforms (FFTs) of ΔD for flapping and rotating compared to flapping alone for the computational (C) and experimental (F) models. Note the peaks at the flapping frequency of 25 Hz, plus and minus the rotation frequency of 3 Hz.

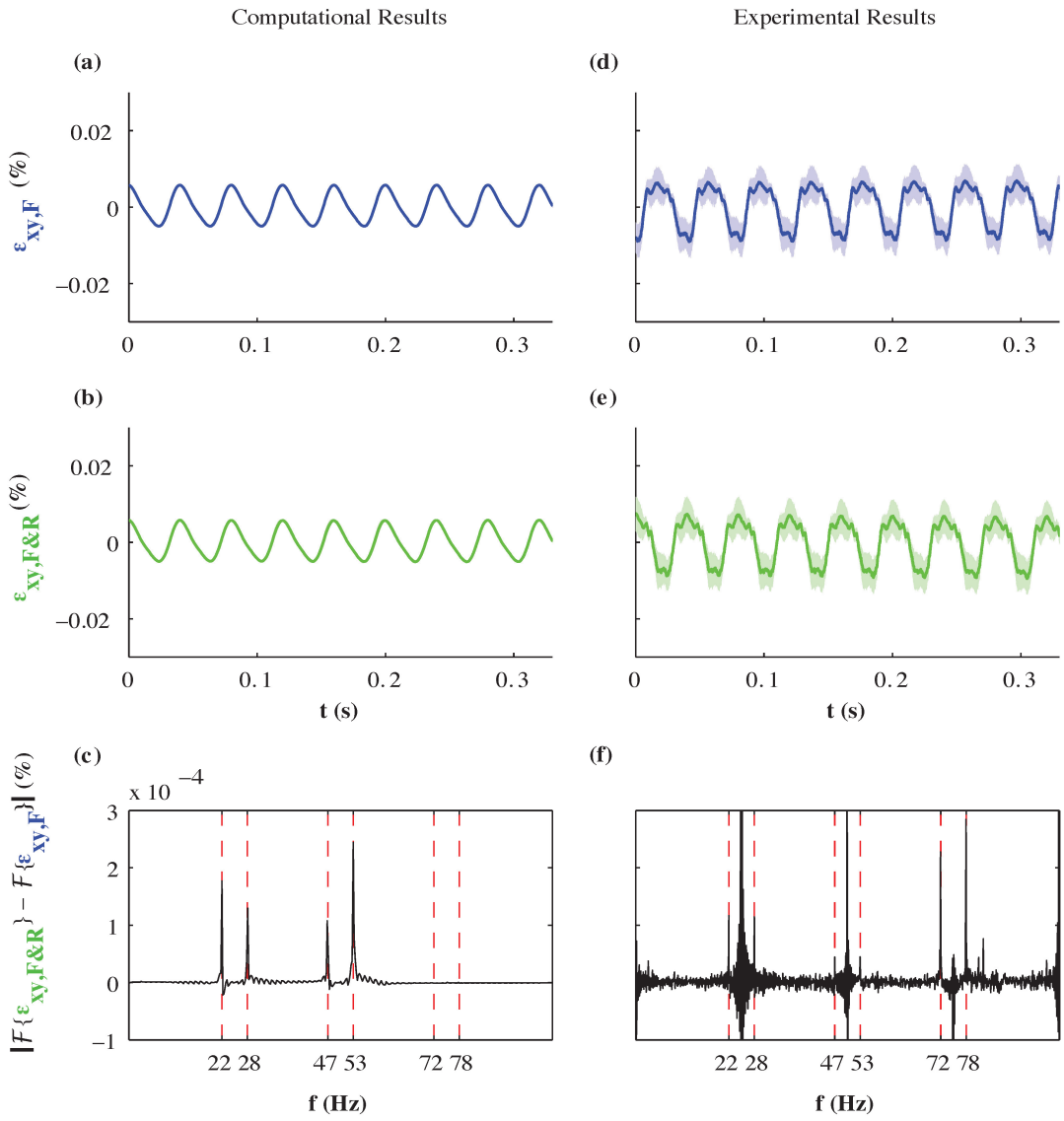

Figure 3.7 The shear strain at the quarter span along the mid chord ε_{xy} versus time, t, for flapping alone (A,D) and flapping and rotating with periodic angular velocity (B,E). The additional subscripts of ε_{xy} are F for flapping alone and $F\&R$ for flapping and rotating. Time domain results for a time-average taken over ten rotation cycles are shown for computational (A-B) and experimental (D-E) models. Shading denotes standard deviation. Frequency domain results of the difference in amplitude of the fast Fourier transforms (FFTs) of ε_{xy} for flapping and rotating compared to flapping alone for the computational (C) and experimental (F) models. Note the peaks at the flapping frequency of 25 Hz, plus and minus the rotation frequency of 3 Hz, and their harmonics.

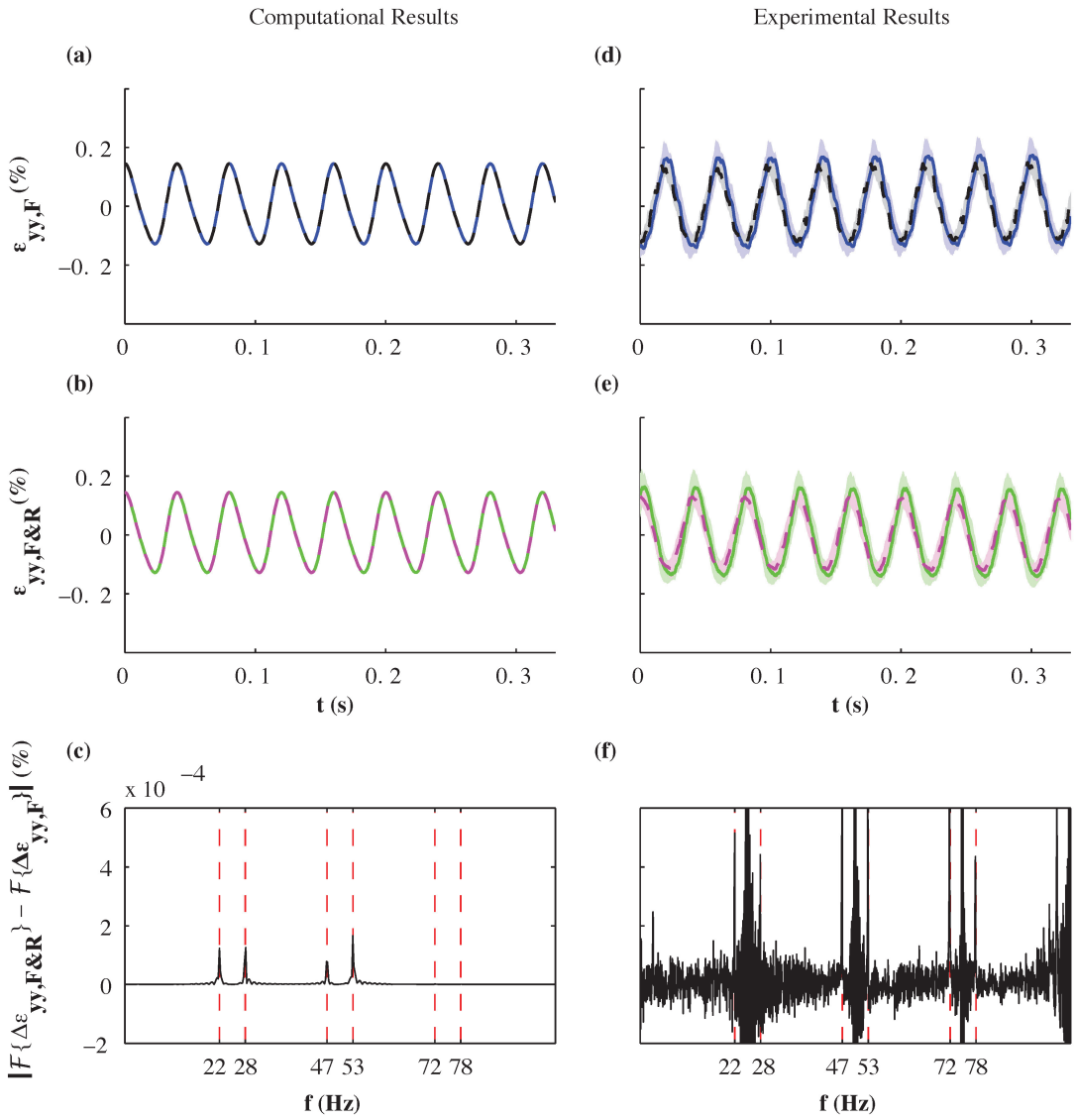

Figure 3.8 The normal strain along the span wise direction, ε_{yy}, on either side of the wing's chord (lift side - solid; right side - dashed) near the base of a model wing versus time, t, for flapping alone (A,D) and flapping and rotating with periodic angular velocity (B,E). The additional subscripts of ε_{yy} are F for flapping alone and $F\&R$ for flapping and rotating. Time domain results for a time-average taken over ten rotation cycles are shown for computational (A-B) and experimental (D-E) models. Shading denotes standard deviation. Frequency domain results of the difference in amplitude of the fast Fourier transforms (FFTs) of the difference between the left and right normal strains, $\Delta\varepsilon_{yy}$, for flapping and rotating compared to flapping alone for the computational (C) and experimental (F) models. Note the peaks at the flapping frequency of 25 Hz, plus and minus the rotation frequency of 3 Hz, and their harmonics.

Chapter 4. VISUAL INFORMATION ATTENUATES WING-MEDIATED MECHANOSENSORY FEEDBACK IN THE HAWKMOTH *MANDUCA SEXTA*

Multimodal sensory integration plays an integral role in helping flying insects maintain stability and reject perturbations. In particular, flies combine visual input with mechanosensory information from the halteres to detect and respond to rotational stimuli. In contrast to the thorough analysis of these sensory streams in flies, there is little work examining if the vast majority of insects, which lack halteres, use similar strategies in flight control. Recent work suggests that wings can inform flying insects of their body dynamics, but how this mechanosensory information combines with the visual system is poorly understood. To understand how multimodal sensory input shapes motor output, I subjected tethered, flying *Manduca sexta* hawkmoths to a wing torsion pitch stimulus *via* magnetic wing perturbations in combination with a visual pattern in dim light and near-total darkness, conditions consistent with the crepuscular periods during which moths are most active. Contrary to prior studies on flies and the moth visual and antennae circuit, I found no difference between moths' response to visual stimulation alone and the combination of visual and wing mechanosensory stimuli. My results show that the visual system is the dominant sensory stream in *Manduca*, that visual information attenuates wing mechanosensory feedback, and the information from the wings is used in a context-dependent manner.

4.1 INTRODUCTION

The control of insect flight is mediated by the interaction of multiple sensory modalities. In particular, insect visual systems play a crucial role in helping animals measure figures against a

moving background (Aptekar et al., 2012; Fox and Frye, 2014; Fox et al., 2014) or avoid obstacles (Bender and Dickinson, 2006a; Tammero and Dickinson, 2002). However, phototransduction chemical cascades result in sensory processing speeds that are far too slow for vision alone to be the sole modality controlling insects' agile maneuvers observed in the wild. By contrast, insect mechanotransduction relies upon the direct coupling of a sensory neuron to the animal's cuticle as well as ionotropic membrane channels (Simmons and Young, 2010). This allows mechanoreceptors to detect mechanical energy imparted by the outside world or due to the animal's own movement with incredible sensitivity and precision (Dickerson et al., 2014; Fox and Daniel, 2008; French, 1988). Thus, insects typically combine visual information with mechanosensory input to control flight.

Most knowledge regarding multimodal sensory integration between visual and mechanosensory inputs comes from work conducted on various Diptera, flies. These insects possess unique mechanosensory organs known as halteres that enable the animal to detect changes in whole-body angular velocity and trigger corrective maneuvers (Dickinson, 1999; Hengstenberg, 1988; Nalbach, 1993; Pringle, 1948). Past work has shown that information from these organs combines with the visual system to control wing steering reflexes in the fruit fly *Drosophila melanogaster* (Sherman and Dickinson, 2004) as well as the activity of neck motor neurons in the blowfly *Calliphora vicina* (Huston and Krapp, 2009). Yet, flies are the only insects that possess halteres and it remains unclear how the vast majority of other flying insects use multimodal sensing to control body dynamics.

Recent studies on the hawkmoth *Manduca sexta* have suggested a role for the antennae as sensors of body dynamics (Hinterwirth and Daniel, 2010; Sane et al., 2007). Further, this mechanosensory input was shown to sum with the visual system to control abdominal flexion

maneuvers during tethered flight (Hinterwirth and Daniel, 2010). However, the measured abdominal flexion response to mechanical stimuli alone, in the form of whole-body rotations, was quite small and suggests that other mechanosensory structures may play a role in flight control.

As halteres are derived from wings, evolution suggests that wings may provide similar mechanosensory input. Indeed, both wings and halteres possess mechanosensory structures known as campaniform sensilla and recent electrophysiological, behavioral, computational, and physical evidence point to a mechanism by which insect wings can detect an animal's angular velocity (Dickerson et al., 2014; Eberle et al., 2015). But in contrast to the thorough analysis of visual and mechanosensory integration in flies, it is unknown if information from the wings combines with the visual system via a similar strategy.

Several possibilities for sensor fusion could occur. For example, the combination of visual and mechanosensory input could sum in a similar manner to the halteres (Sherman and Dickinson, 2004). Alternatively, the combination of the two modalities could lead to an overall attenuated response, as was suggested when antennae-mediated mechanosensory input is combined with the visual system in *Manduca* (Hinterwirth and Daniel, 2010). A third possibility is that the combination of the two inputs does not change relative to the single presentation of one stimulus condition. This result would suggest that under certain circumstances, either visual or mechanosensory input is attenuated, while the other modality dominates flight control.

In this study, I extend the method of Dickerson *et al.* (2014) to explore how the hawkmoth *Manduca* responds to both visual and wing mechanosensory pitch stimuli. Surprisingly, my preliminary results show no difference between moths' responses to the presentation of visual rotation alone and the combination of visual and wing mechanical stimulation. My results

suggest that wing mechanosensory feedback is attenuated in the presence of a strong visual object, even at near-total darkness conditions. These results also suggest that the role of wing mechanosensory is dependent upon the sensory information available from the environment.

4.2 Materials and Methods

4.2.1 *Animals*

Manduca sexta were raised in the Department of Biology at the University of Washington, Seattle. For experiments using a rotating visual stimulus, I used nine male moths 1-3 days post-eclosion. For experiments involving a rotating visual stimulus in near-total darkness, I used four males 1-3 days post-eclosion.

4.2.2 *Wing mechanical stimulus*

I used a pair of Helmholtz coils that have been described previously (Dickerson et al., 2014). I controlled the stepper motor through a custom Arduino script that generated a 20 deg (peak-to-peak), 3 Hz sinusoid about the pitch axis, which was converted into 0.2 deg steps by a micro-step controller (G201, GeckoDrive Inc., Tustin, CA, USA). A previous calibration (Dickerson et al., 2014) of the torque applied to the wings by the magnetic field estimated a torque of 650 nN·m. This torque is within an order of magnitude of the torque experienced by a plate with the same moment inertia as a *M. sexta* wing subject to 10° (amplitude), 3 Hz rotations about the pitch axis.

4.2.3 *Visual stimulus*

The visual stimulus consisted of a half-cylinder with a full-contrast, sinusoidal grating with a spatial frequency of 0.0139 cyc/deg (Figure 4.1A, B). For experiments using a rotating visual stimulus, I mounted the visual drum to the motor that rotated the Helmholtz coils, resulting in

visual motion of 20 deg (peak-to-peak) at 3 Hz. During treatments that tested the combination of visual and wing mechanical perturbation, the visual world rotated down while the torsion experienced by the wings was directed upward. Thus, the combination of visual and wing mechanical perturbation stimulus simulated naturalistic conditions. To track the position of the visual drum when it rotated, I placed a retroreflective marker on the visual drum.

4.2.4 *Animal preparation*

As in previous work on the role of wing mechanosensory feedback (Dickerson et al., 2014), all experiments used the abdominal flexion response that occurs during visual and mechanical pitch rotations (Dyhr et al., 2013; Hinterwirth and Daniel, 2010). The method of moth preparation has been described previously (Dickerson et al., 2014), and below is briefly outlined. I chilled each moth for 20 min in a refrigerator and placed a pair of small rare-earth magnets (mass: 13 mg, diameter: 1.6 mm, height: 0.8 mm; Magcraft NSN0591) between the first and second medial veins of each forewing. I placed the magnets 2.5 mm from the leading edge, such that each wing was in between the pair of attracted magnets. I positioned the magnets to ensure that the polarity was the same for both wings and for all animals. I then glued a ventral tether between the mesothoracic and metathoracic segments and a retroreflective marker (diameter: 3 mm; OptiTrack MCP1125) to the penultimate segment of the abdomen. I dark-adapted each moth for 20 min, but conducted behavioral trials in low light (0.4 lux) conditions and under infrared lighting. I recorded between two to four trials per treatment per moth with a video camera (25 frames s^{-1}, Point Grey Firefly MV, Point Grey Research, BC, Canada).

In the first set of experiments, I subjected moths to two experimental treatments: a rotating visual stimulus alone and the combination of wing mechanical perturbation and visual stimulus. I presented each treatment randomly and only analyzed data from trials that consisted of 8 s of

continuous flight. To test if the visual stimulus impacted the weighting of visual information relative to wing mechanosensory information, I performed a third set of experiments in near total darkness. In these experiments, the visual stimulus rotated with the coils as before, and I compared rotation of the visual drum with and without power being supplied to the Helmholtz coils. I recorded one trial per treatment per moth with a high-speed video camera (500 frames s^{-1}, Phantom v5.1, Vision Research, NJ, USA). Though I only used trials where moths flew for at least 10s, the buffer of the camera was such that I collected approximately 4s of flight per animal.

4.2.5 *Data analysis*

A custom Python script tracked both the visual drum and abdominal marker in real-time for each behavioral trial. This script calculated the angular position of the coils, θ_c, and the angular position of the abdomen, θ_a. I subtracted the means of each time series to remove linear trends from the data, and then performed discrete Fourier transforms of the stimulus and response to calculate the gain of the abdominal reflex at the driving frequency of 3 Hz. I implemented t-tests and two-sample t-tests in Python on the calculated gain values.

4.3 RESULTS

4.3.1 *The combination of visual and wing mechanical information does not impact abdominal reflex gain*

To test if abdominal reflexes mediated by mechanosensory input from the wings are suppressed by input to the visual system, I subjected moths to a visual stimulus that rotated about the pitch axis while supplying a torsional stimulus to the wings (Figure 4.1). I then compared these responses to those of the same moths subjected only to the rotating visual stimulus. Both

the visual stimulus and the wing torsional stimulus rotated at a temporal frequency that is known to elicit strong abdominal motions (Dickerson et al., 2014; Dyhr et al., 2013; Hinterwirth and Daniel, 2010). Moths subjected to the visual stimulus alone exhibited abdominal excursions in the range of ±5°, for a population gain of 0.498 ± 0.307 (mean ± std. dev., n = 28 trials, 9 moths; Figure 4.2A). When I subjected these moths to the combination of visual rotation and a wing torsional stimulus, they exhibited abdominal motions similar to those during just a visual rotating stimulus (gain: 0.504 ± 0.317; Figure 4.2A).

To test for the possibility that an individual moth's response to the combination of visual and mechanosensory input modulated the gain of the abdominal reflex, I calculated the gain ratio for each moth, using the following equation:

$$R = \frac{G_{M+V}}{G_V} - 1$$

where G_{M+V} is the measured gain when moths were subjected to both visual rotation and wing torsional input and G_V is the gain when moths were subjected to visual rotation alone. Thus, values of the gain ratio only had a lower bound of 0, indicating no difference in response between treatments for an individual moth. The combination of visual rotation and wing torsion resulted in an augmented gain of approximately 25% (0.257 ± 0.794; Figure 4.2B). This increased gain during trials with both visual and mechanical stimulation was not statistically significant, however (*t*-test, P = 0.104, n = 28 trials, 9 moths).

4.3.2 *Abdominal reflexes are enhanced in total darkness, but not by mechanical information*

To test if visual input suppresses wing-mediated abdominal flexion responses, I performed experiments where I subjected moths to visual and wing torsion stimuli in near-total darkness. For both treatments, moths exhibited abdominal flexion responses nearly double (± 10°) those

during the aforementioned experiments conducted at 0.3 lx (visual stimulus gain: 1.065 ± 0.238; visual and mechanical gain: 1.091 ± 0.366; mean ± std. dev.; n = 6 trials, 4 moths; Figure 4.2C).

4.4 Discussion

This study was motivated by two main questions. First, given that sensory systems must work in concert, not individually, I tested if input from the visual system interacts with input from the mechanosensory campaniform sensilla embedded in the wings. Second, I examined if it is possible that the presence of a high contrast visual signal attenuates the documented importance of mechanosensory information from the wings. To test each of these questions, I observed moth behavioral responses to the combination of visual and wing mechanosensory inputs, which are known to elicit strong abdominal reflexes when presented individually.

Contrary to previous studies of the relative roles of mechanosensory and visual in *Drosophila* (Sherman and Dickinson, 2003; Sherman and Dickinson, 2004) and *Manduca* (Hinterwirth and Daniel, 2010), the gain of the abdominal flight reflex in *Manduca* is not impacted by concurrent visual and wing mechanosensory input. Further, subjecting moths to both visual and wing mechanosensory stimuli in near total-darkness conditions reveals 1) abdominal reflex gains nearly double those observed in higher light conditions and 2) no differences between trials where moths were subject to visual stimulation only and the combination of visual and mechanical input. Together, these results suggest that any high contrast visual input, even in near total darkness, changes the weighting of visual information relative to wing mechanosensory input such that the visual system becomes the dominant sensory modality for flight control. Thus, the dominant mode of sensorimotor processing during *Manduca* flight is the visual system, but this dominance is dependent on the quality of sensory input.

4.4.1 *Vision is the dominant mode of sensorimotor processing*

Insect flight relies upon both the visual and mechanosensory systems for rejecting external perturbations to achieve stable locomotor performance. The fruit fly *Drosophila* uses information from its visual system along with input from the mechanosensory halteres in a weighted, linear sum that augments reflexes to perturbations compared to the presentation of visual or whole-body rotational stimuli alone (Sherman and Dickinson, 2004). Additionally, the fly flight control system places a greater emphasis on mechanosensory input compared to visual system. Recent evidence from work on *Manduca* has found that the combination of the antennal mechanosensory and visual systems leads to an *attenuation* in flight reflexes (Hinterwirth and Daniel, 2010). There are two additional contrasts between this aspect of *Manduca* flight control circuitry and *Drosophila*: visual and antennal mechanosensory input appear to sum linearly and vision is the more dominant sensory modality (Hinterwirth and Daniel, 2010).

Surprisingly, the results presented in this study suggest that in the presence of *any* visual input change the relative importance of mechanosensory input from the wings. Similar to the results of Hinterwirth and Daniel (Hinterwirth and Daniel, 2010), I found that vision is the dominant sensory stream, though the measured gain for wing torsion alone is over an order of magnitude greater than that for the antennae (Dickerson et al., 2014). I also found that the combination of the visual input and wing torsional input did not change the strength of the abdominal reflex.

That the combination of input from the wings and visual system neither enhanced nor diminished is rather perplexing. Past work on both halteres and insect wings proposed wings to be the evolutionary antecedent to the halteres (Dickerson et al., 2014; Eberle et al., 2015; Pringle, 1948). Perhaps a consequence of the wings being gyroscopic sensor precursors is that the relative

strength of available mehcanosensory information is lower than that of the visual system. The evolution of the haltere led to rapid hypertrophy of dense fields of campaniform sensilla at the structure's base relative to the number of campaniforms on the fly wing (Chan et al., 1998; Pflugstaedt, 1912; Pringle, 1948). Though the central projections of wing afferents are known for the moth *Agrius convolvuli* (Ando et al., 2011), it is unclear how the projections for *Manduca* compare and if these connections provide relevant input. Future work that incorporates comparative morphological and neuroanatomical studies will be able to address if mechanosensory input from the wings of four-winged insects is weaker than that of the halteres. Alternatively, experiments combining whole-body rotation, wing mechanical torsion, and visual stimulation with differing phase relationships would allow further testing of how these two sensory streams work together.

4.4.2 *Flight control processing is context-dependent*

My results suggest that for *Manduca*, while visual input is the dominant sensory stream, that dominance depends on the information available from the environment. Indeed, recent work on flower feeding in *Manduca* suggests that moths will rely on either visual input, mechanosensory information from the proboscis, or both depending to the information available from a flower (Roth *et al., in prep.*). The context-dependence of sensory modalities is not limited to moths. Electric fish tracking a moving shelter are known to switch from relying upon their ability to detect the shelter's electric field in darkness to using their visual system once the shuttle is illuminated (Stamper et al., 2012).

As crepuscular fliers, *Manduca* take advantage of their visual system's extreme contrast sensitivity (Warrant, *personal communication*) to navigate complex environments under poor

visibility. This exceptional ability may explain the lack of difference between treatments where moths were subjected to visual stimulation alone and the combination of visual and wing torsion. The mechanical signal from the wings, though possible to discern through spatiotemporal changes in strain throughout the wingstroke (Eberle et al., 2015), could have been attenuated in the presence of reliable visual signal. This sensitivity to contrast would also explain why the gains observed in all experimental treatments were 50-100% higher than those observed under conditions where wing information was all that was available and the contrast of the Helmholtz coils with the surrounding environment was very low (Dickerson et al., 2014). In these experiments, I used a pattern made of a sinusoidal grating with full contrast. A potentially fruitful future direction would involve testing a range of contrasts to explore the limits of moths' context-dependent reliance on visual information.

4.4.3 *Final thoughts*

I have shown that in the context of insect flight control, vision is the dominant sensory modality, suggesting that the role for wing mechanosensory input that has been previously documented is context-dependent (Figure 4.3). Thus, while insect wings possess the potential to inform an animal of its body dynamics, the availability of visual information influences the extent to which information from the wings is relied upon. This context-dependence may allow flying insects to rapidly switch the sensory modality relied upon when flying through environments in near-total darkness. Future work testing the limits of the wing-mediated flight reflexes and how those are influenced by other sensory systems will allow further insight into how wings serve to inform flying insects of their body dynamics and serve as a point of comparison to the function of halteres, long heralded as the only biological gyroscopic sensors.

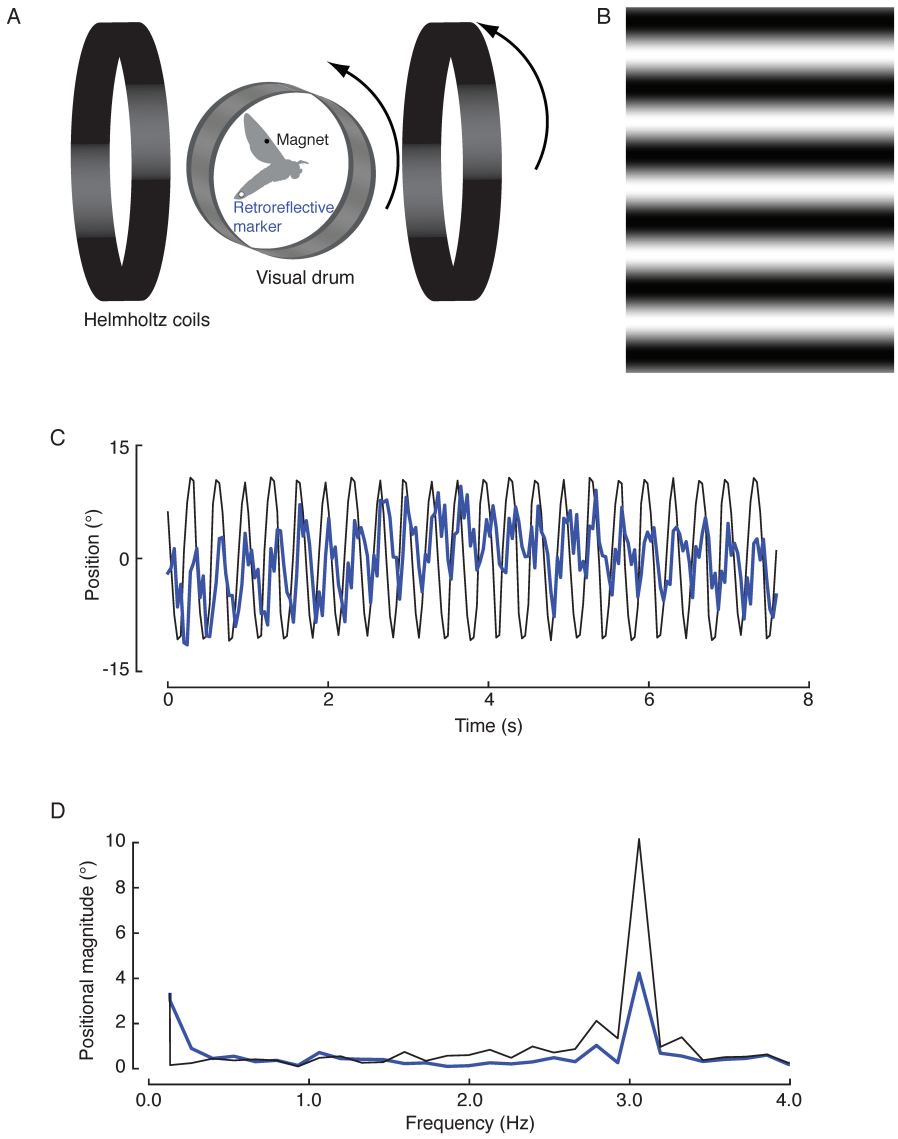

Figure 4.1 Setup to test visual and wing mechanosensory contributions to abdominal flexion response in tethered flight. A) Each moth is tethered with a pair of magnets affixed to each forewing and a retroreflective marker glued to the penultimate abdominal segment. Moths are tasked with flying in front of a visual pattern with a pair of Helmholtz coils. B) The high contrast visual pattern presented to each moth. C) Moth abdominal position (blue) and the position of the Helmholtz coils/visual pattern (black) are tracked as the coils rotate at 3 Hz with an amplitude of 10° when the coils are either powered or unpowered. D) Discrete Fourier Transforms of the sensory input and behavioral output. Note the peaks at 3 Hz.

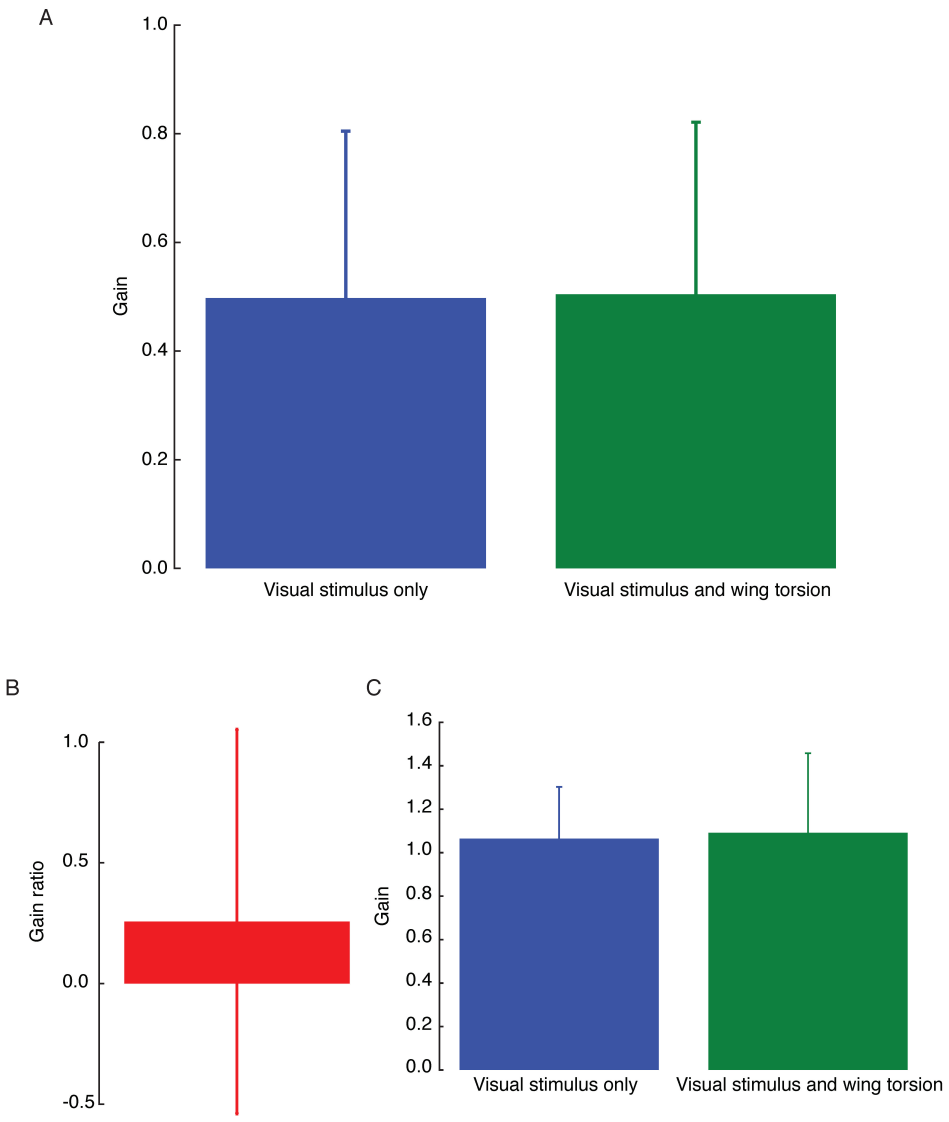

Figure 4.2 Wing-mediated abdominal reflexes are attenuated in the presence of a high contrast visual stimulus. A) Moths subject to a rotating visual stimulus alone at a luminance of 0.3 lx exhibit near identical gains to that of the same moths subject to a rotating visual stimulus and wing torsion via a rotating magnetic field (visual gain: 0.498 ± 0.307; visual and mechanical gain: 0.504 ± 0.317; mean ± std. dev.; n = 28 trials, 9 moths). B) The calculated gain ratio between simultaneous wing and visual stimulation and visual stimulation alone yields no statistically significant difference (0.257 ± 0.794). C) The abdominal reflex gains of moths subject to the same treatments as in panel A, but in near-total darkness, are double that of moths

in brighter conditions (visual gain: 1.065 ± 0.238; visual and mechanical gain: 1.091 ± 0.366). Still, no significant difference exists between the two trials.

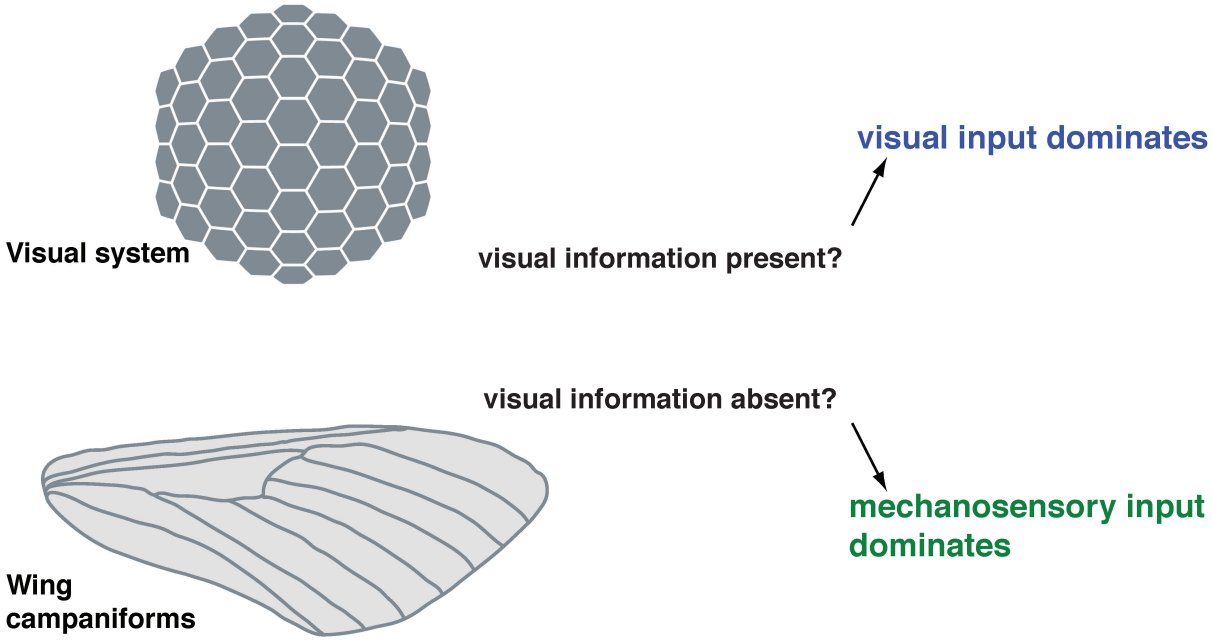

Figure 4.3 Working hypothesis of how the wing mechanosensory and visual systems work together to control abdominal movements during flight. In the presence of any high contrast visual object, visual input dominates flight control circuitry. In total darkness, the flight control circuitry relies upon mechanosensory input from wing campaniform sensilla.

REFERENCES

Ando, N., Wang, H., Shirai, K., Kiguchi, K. and Kanzaki, R. (2011). Central projections of the wing afferents in the hawkmoth, Agrius convolvuli. *Journal of Insect Physiology* **57**, 1518–1536.

Aptekar, J. W., Shoemaker, P. A. and Frye, M. A. (2012). Figure Tracking by Flies Is Supported by Parallel Visual Streams. *Current Biology* **22**, 482–487.

Bender, J. A. and Dickinson, M. H. (2006a). Visual stimulation of saccades in magnetically tethered Drosophila. *Journal of experimental biology* **209**, 3170–3182.

Bender, J. A. and Dickinson, M. H. (2006b). A comparison of visual and haltere-mediated feedback in the control of body saccades in Drosophila melanogaster. *Journal of experimental biology* **209**, 4597–4606.

Bhadbhade, V., Jalili, N. and Nima Mahmoodi, S. (2008). A novel piezoelectrically actuated flexural/torsional vibrating beam gyroscope. *Journal of Sound and Vibration* **311**, 1305–1324.

Borst, A. and Theunissen, F. E. (1999). Information theory and neural coding. *Nat Neurosci* **2**, 947–957.

Brunton B., Eberle A. L., Dickerson B., Brunton S., Kutz J. N., Daniel T. (2014) Sensor placement for sparse sensory decision-making. Salt Lake City, UT: COSYNE. See www.cosyne.org.

Burrows, M. (1975). Monosynaptic connexions between wing stretch receptors and flight motoneurones of the locust. *Journal of experimental biology* **62**, 189–219.

Chan, W. P. and Dickinson, M. H. (1996). Position-specific central projections of mechanosensory neurons on the haltere of the blow fly, Calliphora vicina. *J. Comp. Neurol.* **369**, 405–418.

Chan, W. P., Prete, F. and Dickinson, M. H. (1998). Visual input to the efferent control system of a fly's ‘gyroscope’. *Science* **280**, 289–292.

Chapman, K. M., Duckrow, R. B. and Moran, D. T. (1973). Form and Role of Deformation in Excitation of an Insect Mechanoreceptor. *Nature* **244**, 453–454.

Chapman, K. M., Mosinger, J. L. and Duckrow, R. B. (1979). The role of distributed viscoelastic coupling in sensory adaptation in an insect mechanoreceptor. *Journal of Comparative Physiology A: Sensory, Neural, and Behavioral Physiology* **131**, 1–12.

Chen, J.-S., Chen, J.-Y. and Chou, Y.-F. (2008). On the natural frequencies and mode shapes of dragonfly wings. *Journal of Sound and Vibration* **313**, 643–654.

Cole, E. S. and Palka, J. (1982). The pattern of campaniform sensilla on the wing and haltere of Drosophila melanogaster and several of its homeotic mutants. *J Embryol Exp Morphol* **71**,

41–61.

Combes, S. A. and Daniel, T. L. (2003a). Into thin air: Contributions of aerodynamic and inertial-elastic forces to wing bending in the hawkmoth Manduca sexta. *Journal of experimental biology* **206**, 2999–3006.

Combes, S. A. and Daniel, T. L. (2003b). Flexural stiffness in insect wings. II. Spatial distribution and dynamic wing bending. *Journal of experimental biology* **206**, 2989–2997.

Combes, S. A. and Daniel, T. L. (2003c). Flexural stiffness in insect wings. I. Scaling and the influence of wing venation. *Journal of experimental biology* **206**, 2979–2987.

Daniel, T. L. and Combes, S. A. (2002). Flexible wings and fins: bending by inertial or fluid-dynamic forces? *Integr. Comp. Biol.* **42**, 1044–1049.

Daniel, T., Aldworth, Z., Hinterwirth, A. and Fox, J. (2012). Insect inertial measurement units: Gyroscopic sensing of body rotation. In *Frontiers in Sensing*, pp. 287–297. Vienna: Springer Vienna.

Derham, W. (1711). *Physico-theology*. London: Boyle Lecture for.

Dickerson, B. H., Aldworth, Z. N. and Daniel, T. L. (2014). Control of moth flight posture is mediated by wing mechanosensory feedback. *J. Exp. Biol.*

Dickinson, M. H. (1990a). Comparison of encoding properties of campaniform sensilla on the fly wing. *Journal of experimental biology* **151**, 245–261.

Dickinson, M. H. (1990b). Linear and Nonlinear Encoding Properties of an Identified Mechanoreceptor on the Fly Wing Measured with Mechanical Noise Stimuli. *Journal of experimental biology* **151**, 219–244.

Dickinson, M. H. (1999). Haltere-mediated equilibrium reflexes of the fruit fly, Drosophila melanogaster. *Philos. Trans. R. Soc. Lond., B, Biol. Sci.* **354**, 903–916.

Dickinson, M. H. (2005). The initiation and control of rapid flight maneuvers in fruit flies. *Integr. Comp. Biol.* **45**, 274–281.

Dombrowski, U. (1991). *Dombrowski: Untersuchungen zur funktionellen Organisation... - Google Scholar*.

Dyhr, J. P., Morgansen, K. A., Daniel, T. L. and Cowan, N. J. (2013). Flexible strategies for flight control: an active role for the abdomen. *J. Exp. Biol.* **216**, 1523–1536.

Eberle, A. L., Dickerson, B. H., Reinhall, P. G. and Daniel, T. L. (2015). A new twist on gyroscopic sensing: body rotations lead to torsion in flapping, flexing insect wings. *J R Soc Interface* **12**, 20141088–20141088.

Eberle, A. L., Reinhall, P. G. and Daniel, T. L. (2014). Fluid–structure interaction in

compliant insect wings. *Bioinspir. Biomim.* **9**, 025005.

Elson, R. C. (1987). Flight motor neurone reflexes driven by strain-sensitive wing mechanoreceptors in the locust. *J. Comp. Physiol. A* **161**, 747–760.

Ennos, A. (1988a). The importance of torsion in the design of insect wings. *Journal of experimental biology* **140**, 137–160.

Ennos, A. (1988b). The inertial cause of wing rotation in Diptera. *Journal of experimental biology* **140**, 161–169.

Ennos, A. and Wootton, R. J. (1989). Functional wing morphology and aerodynamics of Panorpa germanica (Insecta: Mecoptera). *Journal of experimental biology* **143**, 267–284.

Fayyazuddin, A. and Dickinson, M. H. (1996). Haltere afferents provide direct, electrotonic input to a steering motor neuron in the blowfly, Calliphora. *J. Neurosci.* **16**, 5225–5232.

Fayyazuddin, A. and Dickinson, M. H. (1999). Convergent mechanosensory input structures the firing phase of a steering motor neuron in the blowfly, Calliphora. *J. Neurophysiol.* **82**, 1916–1926.

Fox, J. L. and Daniel, T. L. (2008). A neural basis for gyroscopic force measurement in the halteres of Holorusia. *Journal of Comparative Physiology A: Sensory, Neural, and Behavioral Physiology* **194**, 887–897.

Fox, J. L. and Frye, M. A. (2014). Figure-ground discrimination behavior in Drosophila. II. Visual influences on head movement. *J. Exp. Biol.*

Fox, J. L., Aptekar, J. W., Zolotova, N. M., Shoemaker, P. A. and Frye, M. A. (2014). Figure-ground discrimination behavior in Drosophila. I. Spatial organization of wing steering responses. *J. Exp. Biol.*

Fox, J. L., Fairhall, A. L. and Daniel, T. L. (2010). Encoding properties of haltere neurons enable motion feature detection in a biological gyroscope. *Proc. Natl. Acad. Sci. U.S.A.* **107**, 3840–3845.

Fraenkel, G. and Pringle, J. W. S. (1938). Halteres of flies as gyroscopic organs of equilibrium. *Nature* **141**, 919–920.

French, A. (1988). Transduction mechanisms of mechanosensilla. *Annu. Rev. Entomol.*

Friedmann, P. P. (2004). Rotary-wing aeroelasticity: Current status and future trends. *AIAA Journal*.

Funk, K., Emmerich, H., Schilp, A., Offenberg, M., Neul, R. and Larmer, F. (1999). A surface micromachined silicon gyroscope using a thick polysilicon layer.pp. 57–60. IEEE.

Gettrup, E. (1965). Sensory mechanisms in locomotion: the campaniform sensilla of the insect

wing and their function during flight. *Cold Spring Harb. Symp. Quant. Biol.* **30**, 615–622.

Gettrup, E. (1966). Sensory regulation of wing twisting in locusts. *Journal of experimental biology* **44**, 1–16.

Gettrup, E. and Wilson, D. M. (1964). THE LIFT-CONTROL REACTION OF FLYING LOCUSTS. *Journal of experimental biology* **41**, 183–190.

Gnatzy, W., Grünert, U. and Bender, M. (1987). Campaniform sensilla of Calliphora vicina (Insecta, Diptera) I. Topography. *Zoomorphology* **106**, 312–319.

Heathcote, S. and Gursul, I. (2007). Flexible Flapping Airfoil Propulsion at Low Reynolds Numbers. *AIAA Journal*.

Hedrick, T. L. (2008). Software techniques for two- and three-dimensional kinematic measurements of biological and biomimetic systems. *Bioinspir. Biomim.* **3**, 034001.

Hedrick T. L., Cheng B., Deng X. Y. (2009). Wingbeat time and the scaling of passive rotational damping in flapping flight. Science 324, 252–255. (doi:10.1126/science.1168431)

Heide, G. (1979). Proprioceptive feedback dominates the central oscillator in the patterning of the flight motoneuron output in Tipula (Diptera). *J. Comp. Physiol. A* **134**, 177–189.

Heide, G. (1983). Neural mechanisms of flight control in Diptera. *BIONA-report* **2**, 35–52.

Hengstenberg, R. (1988). Mechanosensory control of compensatory head roll during flight in the blowfly Calliphora erythrocephala Meig. *Journal of Comparative Physiology A: Sensory, Neural, and Behavioral Physiology* **163**, 151–165.

Hinterwirth, A. J. and Daniel, T. L. (2010). Antennae in the hawkmoth Manduca sexta (Lepidoptera, Sphingidae) mediate abdominal flexion in response to mechanical stimuli. *Journal of Comparative Physiology A: Sensory, Neural, and Behavioral Physiology* **196**, 947–956.

Hinterwirth, A. J., Medina, B., Lockey, J., Otten, D., Voldman, J., Lang, J. H., Hildebrand, J. G. and Daniel, T. L. (2012). Wireless stimulation of antennal muscles in freely flying hawkmoths leads to flight path changes. *PLoS ONE* **7**, e52725.

Hudspeth, A. (1989). How the ear's works work. *Nature* **341**, 397–404.

Huston, S. J. and Krapp, H. G. (2009). Nonlinear integration of visual and haltere inputs in fly neck motor neurons. *J. Neurosci.* **29**, 13097–13105.

Jankauski M. and Shen I. Y. (2014) Dynamic modeling of a rotating insect wing. In Proc. Int. Micro Air Vehicle Conference, Delft, The Netherlands.

Kagawa, Y., Tsuchiya, T. and Kawashima, T. (1996). Finite element simulation of piezoelectric vibrator gyroscopes. *IEEE Trans. Ultrason., Ferroelect., Freq. Contr.* **43**, 509–

518.

Kang, C.-K. and Shyy, W. (2013). Scaling law and enhancement of lift generation of an insect-size hovering flexible wing. *J R Soc Interface* **10**, 20130361.

Kaya, M. O. and Ozdemir Ozgumus, O. (2007). Flexural–torsional-coupled vibration analysis of axially loaded closed-section composite Timoshenko beam by using DTM. *Journal of Sound and Vibration* **306**, 495–506.

Land, M. F. and Collett, T. S. (1974). Chasing behaviour of houseflies (Fannia canicularis). *Journal of Comparative Physiology A: Sensory, Neural, and Behavioral Physiology* **89**, 331–357.

Lehmann, F.-O., Gorb, S., Nasir, N. and Schützner, P. (2011). Elastic deformation and energy loss of flapping fly wings. *J. Exp. Biol.* **214**, 2949–2961.

Melosh R. J. (1963). Basis of derivation of matrices for the direct stiffness method. AIAA J. 1, 1631–1637. (doi:10.2514/3.1869)

Merlin, C., Gegear, R. J. and Reppert, S. M. (2009). Antennal Circadian Clocks Coordinate Sun Compass Orientation in Migratory Monarch Butterflies. *Science* **325**, 1700–1704.

Mittelstaedt, H. (1950). Physiologie des Gleichgewichtssinnes bei fliegenden Libellen. *J. Comp. Physiol. A* **32**, 422–463.

Mountcastle, A. M. and Daniel, T. L. (2010). Vortexlet models of flapping flexible wings show tuning for force production and control. *Bioinspir. Biomim.* **5**, 045005.

Nakata, T. and Liu, H. (2012). Aerodynamic performance of a hovering hawkmoth with flexible wings: a computational approach. *Proc. Biol. Sci.* **279**, 722–731.

Nalbach, G. (1993). The halteres of the blowfly Calliphora I. Kinematics and dynamics. *Journal of Comparative Physiology A: Sensory, Neural, and Behavioral Physiology* **173**, 293–300.

Nalbach, G. and Hengstenberg, R. (1994). The halteres of the blowfly Calliphora II. Three-dimensional organization of compensatory reactions to real and simulated rotations. *J. Comp. Physiol. A* **175**, 695–708.

Norris, A. G., Palazotto, A. N. and Cobb, R. G. (2010). Structural Dynamic Characterization of an Insect Wing.

Pflugstaedt, H. (1912). Die halteren der dipteren. *Zeitschrift fur wissenschaftliche Zoologie* **100**, 1–59.

Pix, W., Nalbach, G. and Zeil, J. (1993). Strepsipteran forewings are haltere-like organs of equilibrium. *Naturwissenschaften* **80**, 371–374.

Pringle, J. W. S. (1948). The gyroscopic mechanism of the halteres of Diptera. *Philos. Trans. R.*

Soc. Lond., B, Biol. Sci. **233**, 347–384.

Pringle, J. W. S. (1957). Insect Flight.

Rayleigh L. (1877). The theory of sound, vol. 1. New York, NY: Macmillan (reprinted 1945 by Dover Publications, New York, NY).

Reddy J.N. (2004). An introduction to the finite element method, 3rd edn. New York, NY: McGraw Hill.

Reissner E. and Stein M. (1951). Torsion and transverse bending of cantilever plates. NACA Technical Note 2369.

Sane, S. P. and McHenry, M. J. (2009). The biomechanics of sensory organs. *Integr. Comp. Biol.* **49**, i8–i23.

Sane, S. P., Dieudonne, A., Willis, M. A. and Daniel, T. L. (2007). Antennal mechanosensors mediate flight control in moths. *Science* **315**, 863–866.

Schäffner, K. H. and Koch, U. T. (1987a). A new field of wing campaniform sensilla essential for the production of the attractive calling song in crickets. *Journal of experimental biology* **129**, 1–23.

Schäffner, K. H. and Koch, U. T. (1987b). Effects of wing campaniform sensilla lesions on stridulation in crickets. *Journal of experimental biology* **129**, 25–40.

Schmidt, J. and Smith, J. (1985). The ultrastructure of the wings and the external sensory morphology of the thorax in female Trichogramma minutum Riley (Hymenoptera: Chalcidoidea: Trichogrammatidae). *Proc. R. Soc. Lond., B, Biol. Sci.* 287–313.

Sherman, A. and Dickinson, M. H. (2003). A comparison of visual and haltere-mediated equilibrium reflexes in the fruit fly Drosophila melanogaster. *Journal of experimental biology* **206**, 295–302.

Sherman, A. and Dickinson, M. H. (2004). Summation of visual and mechanosensory feedback in Drosophila flight control. *Journal of experimental biology* **207**, 133–142.

Simmons, P. and Young, D. (2010). Nerve Cells and Animal Behaviour - Peter Simmons, David Young - Google Books.

Smith, G. L., Bedair, S. S., Schuster, B. E., Nothwang, W. D., Pulskamp, J. S., Meyer, C. D. and Polcawich, R. G. (2012). Biologically inspired, haltere, angular-rate sensors for micro-autonomous systems. In (eds. George, T., Islam, M. S., and Dutta, A., pp. 83731K–83731K–13. SPIE.

Stamper, S. A., Roth, E., Cowan, N. J. and Fortune, E. S. (2012). Active sensing via movement shapes spatiotemporal patterns of sensory feedback. *J. Exp. Biol.* **215**, 1567–1574.

Tammero, L. F. and Dickinson, M. H. (2002). The influence of visual landscape on the free flight behavior of the fruit fly Drosophila melanogaster. *J. Exp. Biol.* **205**, 327–343.

Thakkar, D. and Ganguli, R. (2004). Helicopter vibration reduction in forward flight with induced-shear based piezoceramic actuation. *Smart Mater. Struct.* **13**, 599–608.

Theobald, J. C., Warrant, E. J. and O'Carroll, D. C. (2010). Wide-field motion tuning in nocturnal hawkmoths. *Proc. Biol. Sci.* **277**, 853–860.

Thompson R. A., Wehling M. F., Evers J. H., Dixon W. E. (2008). Body rate decoupling using haltere mid-stroke measurements for inertial flight stabilization in Diptera. J. Comp. Physiol. A 195, 99–112. (doi:10.1007/s00359-008-0388-1)

Vanella, M., Fitzgerald, T., Preidikman, S., Balaras, E. and Balachandran, B. (2009). Influence of flexibility on the aerodynamic performance of a hovering wing. *Journal of experimental biology* **212**, 95–105.

Veers, P., Lobitz, D. and Bir, G. (1998). Aeroelastic tailoring in wind-turbine blade applications.

Viollet, S. and Zeil, J. (2013). Feed-forward and visual feedback control of head roll orientation in wasps (Polistes humilis, Vespidae, Hymenoptera). *J. Exp. Biol.* **216**, 1280–1291.

Voss, R., Bauer, K., Ficker, W., Gleissner, T., Kupke, W., Rose, M., Sassen, S., Schalk, J., Seidel, H. and Stenzel, E. (1997). Silicon angular rate sensor for automotive applications with piezoelectric drive and piezoresistive read-out.pp. 879–882. IEEE.

Walker, R. G., Willingham, A. T. and Zuker, C. S. (2000). A Drosophila mechanosensory transduction channel. *Science* **287**, 2229–2234.

Walker, S. M., Thomas, A. L. R. and Taylor, G. K. (2009). Deformable wing kinematics in the desert locust: how and why do camber, twist and topography vary through the stroke? *J R Soc Interface* **6**, 735–747.

Wilson, D. M. (1961). The central nervous control of flight in a locust. *J. Exp. Biol.* **38**, l–490.

Wootton, R. J. (1981a). Support and Deformability in Insect Wings. *Journal of Zoology* **193**, 447–468.

Wootton, R. J. (1981b). Support and deformability in insect wings. *Journal of Zoology* **193**, 447–468.

Wootton, R. J. (1992). Functional morphology of insect wings. *Annu. Rev. Entomol.* **37**, 113–140.

Wootton, R. J. (1993). Leading edge section and asymmetric twisting in the wings of flying butterflies (Insecta, Papilionoidea). *Journal of experimental biology* **180**, 105–117.

Wu, W. C., Wood, R. J. and Fearing, R. S. (2002). Halteres for the micromechanical flying insect.pp. 60–65. IEEE.

Yen, S.-C., Baker, J. and Gray, C. M. (2007). Heterogeneity in the responses of adjacent neurons to natural stimuli in cat striate cortex. *J. Neurophysiol.* **97**, 1326–1341.

Young, J., Walker, S. M., Bomphrey, R. J., Taylor, G. K. and Thomas, A. L. R. (2009). Details of insect wing design and deformation enhance aerodynamic function and flight efficiency. *Science* **325**, 1549–1552.

Zacwilichowski, J. (1931). *Über die Innervierung und die Sinnesorgane der Flügel der Insekten, II. Teil*. Bull. Acad. pol. Cl. Math. Nat.

Zill, S. N. and Moran, D. T. (1981). The exoskeleton and insect proprioception. I. Responses of tibial campaniform sensilla to external and muscle-generated forces in the American cockroach, Periplaneta americana. *Journal of experimental biology* **91**, 1–24.

Zill, S. N., Moran, D. T. and Varela, F. G. (1981). The Exoskeleton and Insect Proprioception: II. Reflex Effects of Tibial Campaniform Sensilla in the American Cockroach, Periplaneta Americana. *Journal of experimental biology* **94**, 43–55.

APPENDIX A

```
%%Script to characterize stimulus by computing the rotation of the Helmholtz coil to make sure it is
%truly sinusoidal during a 10 sec trial at 3 Hz. Created 1/28/13 by BHD. Modified on 1/30/13 to
%do the entire analysis for a single moth just using three points. This also calculates FFTs of the
%stim and response, as well as the gain and phase.
%P1: point on tether, P2: abdomen, P3: LED.

p1=[data(:,1) data(:,2)];
p2=[data(:,3) data(:,4)];
p3=[data(:,5) data(:,6)];

abdo_vec=zeros(length(p1),2);
coil_vec=zeros(length(p1),2);


abdo_vec(:,1)=(p2(:,1)-p1(:,1));
abdo_vec(:,2)=(p2(:,2)-p1(:,2));

abdo_angle=atan2(abdo_vec(:,2),abdo_vec(:,1));
abdo_angle=unwrap(abdo_angle);
abdo_angle=-(rad2deg(abdo_angle)); %flipped abdo response to Jon's convention

coil_vec(:,1)=(p3(:,1)-p1(:,1)); %Calculate x and y vectors
coil_vec(:,2)=(p3(:,2)-p1(:,2));

coil_angle=atan2(coil_vec(:,2),coil_vec(:,1));
coil_angle=unwrap(coil_angle);
coil_angle=rad2deg(coil_angle);




Fs=100;
t=0:1/Fs:10;
time=1:1000;


% cyc_len=33;
% coil_stim_chunk=zeros(30,33);
% abdo_stim_chunk=zeros(30,33);
```

```
% %current_time=[44 77 111 144 177 211 244 277 311 344 377 411 444 477
511 544 577 611 644 677 711 744 777 811 844 877 911 944 977];
% current_time=[63 96 130 163 196 230 263 296 330 363 396 430 463 496
530 563 596 630 663 696 730 763 796 830 863 896 930 963 996];
% for i=1:length(current_time)
%    stim_chunk(i,:)=coil_angle(current_time(i)-cyc_len+1:current_time(i));
%                                    abdo_stim_chunk(i,:)=abdo_angle(current_time(i)-
cyc_len+1:current_time(i));
% end
% cyc_avg=mean(stim_chunk,1);
% cyc_std=std(cyc_avg);
% abdo_cyc_avg=mean(abdo_stim_chunk,1);
% abdo_std=std(abdo_cyc_avg);


figure
subplot(2,1,2)
plot(t(1:1000),coil_angle-coil_angle(1))
%plot(t(1:33),cyc_avg-cyc_avg(1)-10)
xlabel('Time (s)')
ylabel('Coil angle (∞)')
subplot(2,1,1)
%[l,p]= boundedline(t(1:33),abdo_cyc_avg-abdo_cyc_avg(1),abdo_std,'k')
 plot(t(1:1000),abdo_angle-abdo_angle(1),'r')
xlabel('Time (s)')
ylabel('Wing torsion angle (∞)')
%ylim([-10 10])

%compute FFTs of the stimulus and response, then calculate gain/phase
L=1000;
NFFT = 2^nextpow2(L);
THETA = fft(detrend(coil_angle-mean(coil_angle)),NFFT)/L;
abs_THETA=abs(THETA);
THETA_imag=imag(THETA);
f = Fs/2*linspace(0,1,NFFT/2);
coil_fft=2*abs_THETA(1:NFFT/2);
figure
subplot(2,1,2)
 plot(f(1:96),coil_fft(1:96))
 xlabel('Frequency (Hz)')
 ylabel('Positional magnitude (∞)')
 ylim([0 10])
ALPHA = fft(detrend(abdo_angle-mean(abdo_angle)),NFFT)/L;
abs_ALPHA=abs(ALPHA);
ALPHA_imag=imag(ALPHA);
abdo_fft=2*abs_ALPHA(1:NFFT/2);
```

```
subplot(2,1,1)

plot(f(1:96),abdo_fft(1:96),'b')
xlabel('Frequency (Hz)')
ylabel('Positional magnitude (∞)')
[drive_stim,ind]=max(THETA(1:NFFT/2));
resp=ALPHA(ind);
gain=abs(resp/drive_stim)
phase_angle=rad2deg(angle(resp/drive_stim))
%gain=resp/drive_stim
%%
cyc_len=33;
coil_stim_chunk=zeros(30,33);
current_time=[33 67 100 133 167 200 233 267 300 333 367 400 433 467 500
533 567 600 633 667 700 733 767 800 833 867 900 933 967 1000];
for i=1:length(current_time)
   stim_chunk(i,:)=coil_angle(current_time(i)-cyc_len+1:current_time(i));
end
cyc_avg=mean(stim_chunk,1);
cyc_std=std(cyc_avg);
```

APPENDIX B

```
import numpy as np

# we assume that the supplied csv file will have two columns, containing time in
# the first column and position in the second. position should be normalized
# position, i.e. ranging between [-1,1]
filename='sumofsines.csv'

# desired output amplitude of motor motion, in degrees
amplitude=20
# stepper motor step resolution (standard is 1.8 for 200 deg/rev, if
# microstepping is enabled this becomes, e.g.,  0.18)
step_resolution=0.18

# load record array from file
ss = np.loadtxt(filename, delimiter=',', dtype=[('t', 'f4'), ('pos', 'f4')])

# convert position into step number, where step 0 is the origin.
bin_pos = np.floor((amplitude*ss['pos'] + 0.5*step_resolution) / step_resolution)

# now find where the motor actually needs to produce a step, i.e. where the
# change in bin_pos is not zero.

steps = np.diff(bin_pos)

time = ss['t'][np.argwhere(steps!=0)].flatten()

# step directions are -1 and +1, so renormalize so that direction is either 0 or
# 1 (i.e. low/high)
direction = (0.5*(steps[np.argwhere(steps!=0)].flatten() + 1)).astype(int)

# now produce a file for inclusion into an arduino project.

f = open('sumofsines.h', 'w')
f.write('int num_steps = {};\n'.format(len(time)))
f.write('float step_time[]  = { ')
for t in time[:-1]:
   f.write('{:.3f}, '.format(t))
f.write('{:.3f} }};\n'.format(time[-1]))

f.write('int step_direction[] = { ')
for d in direction[:-1]:
   f.write('{:d}, '.format(d))
f.write('{:d} }};\n'.format(direction[-1]))
```

```
f.close()
```

APPENDIX C

```
import os
import numpy as np
import cv2
import glob
import pandas as pd

# Change the following line to the full path of the directory where your images
# are:
imdir = '/Users/bradleydickerson/Documents/projects/chap 4/629_v/'
# Find all the files in that directory with a .jpeg extension, return a sorted
# list of files
imglist = sorted(glob.glob(imdir+'*.jpeg'))

# Set to false if you do not want to spawn a window showing tracker progress
show_tracks = True

# Size of images to be tracked (note that this is (height, width))
#im_size = (600,800)

im_size = (768,1024)
# Threshold values for tracking, out of a max value of 255 -- set these values
# to just below the pixel values of the thing you want to track; in the example
# video the abdomen was a significantly brighter marker than the coil marker.
abdo_threshval = 200
mark_threshval = 120

# ABDOMEN REGION OF INTEREST
# Define the image
ab_mask = np.zeros(im_size, dtype=np.uint8)
```

```
# Define polygon region of interest for the abdomen
# Edit as necessary
#ab_center = (400,270)
ab_center = (512,350)
ab_rmax = (220,220)
ab_rmin = (120,120)
ab_angle = 180
ab_ang_min = -45
ab_ang_max = 45
ab_degrees_per_segment = 5

outer_line = cv2.ellipse2Poly(ab_center, ab_rmax, ab_angle, ab_ang_min, ab_ang_max,
    ab_degrees_per_segment)
inner_line = cv2.ellipse2Poly(ab_center, ab_rmin, ab_angle, ab_ang_min, ab_ang_max,
    ab_degrees_per_segment)
ab_roi_poly = np.append(outer_line, inner_line[::-1]).reshape(-1,2)
cv2.fillConvexPoly(ab_mask, ab_roi_poly, 1)

# MARKER REGION OF INTEREST
# Define polygon region of interest for the abdomen
# Edit as necessary
ma_mask = np.zeros(im_size, dtype=np.uint8)
#ma_center = (400,300)
ma_center = (512,384)
ma_rmax = (500,500)
ma_rmin = (400,400)
ma_angle = 0
ma_ang_min = -45
ma_ang_max = 45
```

```
ma_degrees_per_segment = 5

outer_line = cv2.ellipse2Poly(ma_center, ma_rmax, ma_angle, ma_ang_min,
ma_ang_max,
    ma_degrees_per_segment)
inner_line = cv2.ellipse2Poly(ma_center, ma_rmin, ma_angle, ma_ang_min,
ma_ang_max,
    ma_degrees_per_segment)
ma_roi_poly = np.append(outer_line, inner_line[::-1]).reshape(-1,2)
cv2.fillConvexPoly(ma_mask, ma_roi_poly, 1)


tracks = []

for img_path in imglist:
  # Strip out the frame file, remove the '.jpeg' extension
  frame = os.path.basename(img_path)[:-5]
  # Read in the raw image (we'll use this for display later)
  raw = cv2.imread(img_path)
  # Convert raw image to grayscale
  img = cv2.cvtColor(raw, cv2.COLOR_RGB2GRAY)

  # Make two new images for analysis by masking the grayscale image with the
  # masks we made for the abdomen and the marker
  abdo_img = cv2.bitwise_and(img,img, mask=ab_mask)
  mark_img = cv2.bitwise_and(img,img, mask=ma_mask)

  # Threshold the abdomen image using the abdoment threshold value, obtaining
  # a binary image
  abdo_thresh = cv2.threshold(abdo_img, abdo_threshval, maxval=1,
      type=cv2.THRESH_BINARY)[1]
```

```
  i=0
  while max(abdo_thresh.flatten()) == 0:
    print i,
    i+=1
    abdo_thresh=cv2.threshold(abdo_img, abdo_threshval-10*i, maxval=1,
type=cv2.THRESH_BINARY)[1]#lower the threshold and print
    #the number of times the threshold is lowered

  # Calculate the moments of the image -- note that this will only work if the
  # abdomen marker is the ONLY thing in the thresholded ROI
  abdo_moments = cv2.moments(abdo_thresh)
  abdo_centroid_x = abdo_moments['m10']/abdo_moments['m00']
  abdo_centroid_y = abdo_moments['m01']/abdo_moments['m00']

  # Go through the same process for the coil marker
  mark_thresh = cv2.threshold(mark_img, mark_threshval, maxval=1,
      type=cv2.THRESH_BINARY)[1]
  mark_moments = cv2.moments(mark_thresh)
  mark_centroid_x = mark_moments['m10']/mark_moments['m00']
  mark_centroid_y = mark_moments['m01']/mark_moments['m00']

  mark_theta = np.arctan2(mark_centroid_y-ma_center[1], mark_centroid_x-
ma_center[0])
  abdo_theta = np.arctan2(abdo_centroid_y-ab_center[1], abdo_centroid_x-
ab_center[0])

# Eatai Test
  #mark_theta = np.arctan2(-1*(mark_centroid_y-ma_center[0]),
mark_centroid_x-ma_center[1])
  #abdo_theta = np.arctan2(-1*(abdo_centroid_y-ab_center[0]),
abdo_centroid_x-ab_center[1])
```

```
##


  mark_theta=np.degrees(mark_theta)
  abdo_theta=-(np.degrees(abdo_theta))



  #t=img_path

  # Append a dictionary to the tracks list containing the relevant info --
  # we'll turn this into a Pandas dataframe at the end.
  tracks.append({'frame': frame, 'abdo_x': abdo_centroid_x,
     'abdo_y': abdo_centroid_y, 'marker_x': mark_centroid_x,
     'marker_y': mark_centroid_y, 'marker_theta': mark_theta,
     'abdominal_theta':abdo_theta})

  # If you don't need to see the process happening, feel free to set
  # show_tracks to False at the beginning of the script.
  if show_tracks:

     # Draw a circle at the abdomen centroid on the raw image
     cv2.circle(raw, (int(abdo_centroid_x), int(abdo_centroid_y)), 5,
          (255,0,0))
     # Draw the abdoment region of interest
     cv2.polylines(raw, [ab_roi_poly], True, (255,0,0), 2)
     # Mark the marker centroid
     cv2.circle(raw, (int(mark_centroid_x), int(mark_centroid_y)), 5,
          (0,0,255))
     # Draw the marker ROI
     cv2.polylines(raw, [ma_roi_poly], True, (0,0,255), 2)
```

```
        # Show the image in a window
        cv2.imshow('Raw Image', raw)
        # Wait one millisecond before going onto the next frame (increase this
        # value if you want it to go slower, or change it to zero if you want to
        # step through the video frame by frame to check progress
        cv2.waitKey(1)

# Assemble a data frame from the tracks using Pandas
tracks = pd.DataFrame(tracks)

# Uncomment this line to save the data to a CSV file.
#tracks.to_csv('track_data.csv', index=False)
```

VITA

Brad Dickerson was born and raised in central New Jersey, first in the capital, Trenton, then in nearby Lawrence. He grew up on a steady diet of trips to local science museums, *National Geographic for Kids*, and spending the rest of his free time imagining different worlds through Lego. By the age of eight, he announced his intention to become a marine biologist, but this dream faded during a jaded adolescence. During his first year at Swarthmore College, he attended a guest lecture and learned for the first time how a professor's time was spent at other, larger schools. This sparked a desire to conduct research firsthand. After working on sea squirts at Friday Harbor with Dr. Molly Jacobs and Dr. Richard Strathmann, and examining caterpillar development with Dr. Lynn Riddiford, Brad determined that a life of research was right for him. After a brief detour in informal education at the Museum of Science in Boston, Brad began working on insect flight control in the lab of Dr. Ty Hedrick at UNC Chapel Hill. Soon after, Brad moved out to Seattle to work in the Daniel lab, where he came to appreciate the power that engineering techniques can bring to biology and the pregnant pauses post-puns.